E.O. Paton Electric Welding Institute of the National Academy of Sciences of Ukraine

International Scientific-Technical and Production Journal

The Paton WELDING JOURNAL

Issue 02 2018

Published Monthly Since 2000

English translation of the monthly «Avtomaticheskaya Svarka» (Automatic Welding) journal published in Russian since 1948

Address
E.O. Paton Electric Welding Institute,
International Association «Welding»
11 Kazimir Malevich Str. (former Bozhenko Str.),
03150, Kyiv, Ukraine
Tel.: (38044) 200 60 16, 200 82 77
Fax: (38044) 200 82 77, 200 81 45
E-mail: journal@paton.kiev.ua
www.patonpublishinghouse.com

State Registration Certificate
KV 4790 of 09.01.2001
ISSN 0957-798X
DOI: http://dx.doi.org/10.15407/tpwj

Subscriptions
$348, 12 issues per year,
air postage and packaging included.
Back issues available.

CONTENTS

SCIENTIFIC AND TECHNICAL

Taraborkin L.A. and *Golovko V.V.* Calculation model of formation of nonmetallic inclusions of multilayer morphology in weld metal 2

Markashova L.I., Poznyakov V.D., Shelyagin V.D., Berdnikova E.N., Bernatsky A.V. and *Alekseenko T.A.* Effect of metal structure on service properties of high-strength steel welded joints produced using different methods of welding 7

Knysh V.V., Solovej S.A., Nyrkova L.I. and *Miryanin V.N.* Influence of corrosion damage on cyclic life of butt welded joints strengthened by high-frequency mechanical peening 14

Stefaniv B.V. and *Sabadash O.M.* Effect of structure of joint zone of diamond layer with hard-alloy substrate of brazed cutters on their service life 19

INDUSTRIAL

Kuzmenko G.V., Taganovsky V.M. and *Sidorenko V.L.* Electric arc welding and surfacing in repair of rails of Kyiv underground 23

Poznyakov V.D., Demchenko Yu.V., Denisenko A.M., Zhuk G.V. and *Kozyrev V.B.* Application of welding for restoration of cast iron railing of the Kotzebue Bridge in Odessa 26

Borisov Yu.S., Vojnarovich S.G., Kislitsa A.N., Kalyuzhny S.N. and *Glukhovsky V.Yu.* Application of the method of microplasma spraying for manufacturing resistance heating element 33

Kuskov Yu.M., Soloviov V.G., Osechkov P.P. and *Osin V.V.* Electroslag surfacing of billet end faces with application of consumable and nonconsumable electrodes 38

INFORMATION

Laser Technology and Equipment for Manufacture of Multilayer Bellows 42

Unit for Manual Laser Welding 43

Laser Welding of Body Elements with Loose Edges 43

DOI: http://dx.doi.org/10.15407/tpwj2018.02.01

CALCULATION MODEL OF FORMATION OF NONMETALLIC INCLUSIONS OF MULTILAYER MORPHOLOGY IN WELD METAL

L.A. TARABORKIN and **V.V. GOLOVKO**
E.O. Paton Electric Welding Institute of the NAS of Ukraine
11 Kazimir Malevich Str., 03150, Kyiv, Ukraine. E-mail: office@paton.kiev.ua

The objective of the work was development of a calculation model for practical prediction of the kinetics of formation of multicomponent endogenous nonmetallic inclusions in the weld metal. The proposed mathematical model is a nonstandard nonlinear boundary problem for a system of diffusion equations with the specific condition on the moving melt-inclusion interphase, and it allows for the kinetics and heterogeneity of the process under the conditions of the real thermal cycle of welding. The calculation program developed as a computer realization of the constructed model allows evaluating in a computer experiment the size and composition of endogenous nonmetallic oxide inclusions, depending on concentration and thermal conditions in the weld pool. 10 Ref., 2 Figures.

Keywords: *arc welding, weld pool, nonmetallic inclusions, mathematical model, prediction*

Nonmetallic inclusions are a natural component of the structure of any steel, having a significant role in various processes and phenomena, both in its production and in subsequent service [1–3].

Mathematical models for prediction of the composition, size and quantity of nonmetallic inclusions, available in scientific publications, are characterized by that in their attempts to simplify their mathematical and computer realization, the authors have to make certain assumptions that do not completely correspond to the features of physico-chemical and thermo-physical processes in welding [4, 5]. In particular, we are talking about the need to allow for high gradients of temperatures and concentrations, which accompany formation of the weld, as well as an essential nonstationarity and heterogeneity of the respective processes. The above features can be taken into account, using for mathematical model definition the equations of the type of reaction diffusion with addition of a specific condition on the moving surface of the formed nonmetallic inclusion, what exactly was done in this work.

Physico-chemical description of the process. The mathematical model was based on the following physico-chemical description of the process of nonmetallic inclusion formation in the weld metal:

1) range of considered temperatures at cooling of weld pool metal is from 2300 to 1670 K, in keeping with the real thermal cycle of welding (upper limit of the temperature range corresponds to the lowest temperature of formation of Al_2O_3 aluminium oxide, which is the most high-melting compound compared to other components of nonmetallic inclusions in the specified system);

2) at the initial moment of time the deoxidizer elements (Al, Ti, Si, Mn, etc.) are homogeneously dissolved in the melt;

3) nonmetallic inclusion nuclei have the shape of a sphere (with initial radius equal to critical radius calculated through the free energy of formation) and are uniformly distributed in the melt volume;

4) inclusion formation begins in the liquid metal of the weld pool and goes on in the two-phase zone, inclusion growth occurring in the diffusion cell of a certain size by the reactive diffusion mechanism, namely reagents (oxygen and deoxidizer elements) are transported through diffusion transfer to the inclusion surface, on which the respective chemical reaction of their interaction runs, and reaction products adsorb on the above surface;

5) probability of formation of inclusions of a certain composition depends on their melting temperature and formation energy so that unlike the known models, different sets of chemical reactions are considered within certain temperature subranges, and the composition of the melt metal matrix changes, respectively;

6) diffusion regions of growing inclusions do not overlap;

7) at each moment of time during the entire process a thermodynamically equilibrium state is in place on «inclusion-melt» interface;

8) temperature conditions of the process are assigned as functional dependence of temperature on time variable.

Formulation of the mathematical model. In order to formulate the respective mathematical model by this physico-chemical description, we will introduce the following designations:

N is the total number of reagent elements (oxygen, deoxidizers, etc.) in the system;

i is the number of the considered chemical element;

C_i is the content (concentration) of the i-th element in the melt, mole/cm^3;

M_i is the molecular mass of the i-th element;

D_i is the coefficient of diffusion of the i-th element in the melt, mole/(cm^2·s);

t is the time variable, s;

r is the geometrical variable in the spherical system of coordinates;

$a(t)$ is the current radius of the inclusion at moment of time t, cm;

T is the temperature as a function of time, $T = T(t)$, K;

r_m is the size of the diffusion cell related to volume fraction V_f and average volume of inclusions V_m, cm

$$r_m = \frac{1}{2}\sqrt[3]{\frac{V_m}{V_f}}.$$

We will describe the volume mass transfer (beyond the inclusion) by Fick's diffusion equation, which has the following form in the spherical system of coordinates:

$$\frac{\partial C_i(r,t)}{\partial t} = \frac{1}{r^2}\frac{\partial}{\partial r}\left(D_i(T)r^2\frac{\partial C_i(r,t)}{\partial r}\right), \quad a(t) < r < r_m; \tag{1}$$

on the interface the reagent concentration is calculated as equilibrium value $C_{i,\text{eq}} = f\left(C_j\big|_{r=a(t)}, T(t)\right)$, in keeping with assumption 4):

$$C_i(r,t)\big|_{r=a(t)} = C_{i,\text{eq}}; \tag{2}$$

on the diffusion cell boundary the substance flow is absent that corresponds to the following equation:

$$\frac{\partial C_i(r,t)}{\partial r}\bigg|_{r=r_m} = 0; \tag{3}$$

during the inclusion growth its radius becomes greater due to simultaneous precipitation of products of the respective chemical reaction on the inclusion surface:

$$\frac{1}{3}\frac{d}{dt}\left(\rho a^3(t)\right) = a^2(t)k\left(C_{j,\text{eq}}, T\right)\times \times\sum_{i=1}^{N} X_i(T)M_iD_i(T)\frac{\partial C_i(r,t)}{\partial r}\bigg|_{r=a(t)}, \tag{4}$$

where $X_i(T)$ is the characteristic function, which actually determines the set of oxides, which can be present in the nonmetallic inclusions in each temperature range:

$$X_i(T) = \begin{cases} 0, & T > T_i, \\ 1, & T \le T_i, \end{cases}$$

where T_i denotes the melting temperature of i-th oxide. Thus, assuming that $T_1 > T_2 > T_3 > T_4 > ...$, we obtain that at temperature below T_2 the nonmetallic inclusion contains just the first oxide; at further lowering of temperature to T_3 the nonmetallic inclusion will form from both the first and second oxides; in the next temperature range it will form already from three oxides, and so on (note that such a pattern corresponds to the one described in monograph [1]); coefficient $k(C_{j,\text{eq}}, T)$ depends on the current concentration state at the inclusion surface, and it can be determined at any moment of time, on condition of an equilibrium redistribution of the substance transported to the surface of the inclusion between the metal and slag phases.

The initial condition consists in that the reagent concentration fields are spatially homogeneous (in the area between the inclusion surface and boundary of the diffusion cell):

$$C_i(r,t)\big|_{t=0} = C_{i,0}, \quad a(0) < r < r_m, \tag{5}$$

- here, the initial conditions are calculated by a separate algorithm, which allows for the actual welding conditions;
- initial radius of the inclusion, according to assumption 3), is equal to the nucleus critical radius:

$$a(0) = r_{\text{crit}}\left(C_{i,0}, T(0)\right). \tag{6}$$

Thus, the mathematical model of nonmetallic inclusion formation is formulated as a nonlinear boundary problem (1)–(6) for a system of equations of diffusion type in a region with moving boundary, being a reactive diffusion problem in its sense.

A distinctive feature of this model is allowing for the nonstationarity of the process under the conditions of multicomponent nature of the system, in which inclusions form. Moreover, owing to nonstandard condition (4) on a moving surface of the growing inclusion, it is possible to avoid the technically difficult determination of constants of the mentioned reaction rates, the values of which are also strongly dependent on temperature.

On the other hand, boundary condition (4) on the interface makes it necessary to calculate the equilibrium state of the multicomponent system, which can be presented as that made of two solutions, namely metal and slag one.

An important stage of numerical modelling of the process of formation of endogenous nonmetallic inclusions is calculation of the initial content of alloying elements in the weld pool. Algorithm of this calculation is presented in detail in [6]. The above-mentioned algorithm is based on the model of alloying elements transition into the weld pool and the weld for submerged-arc welding and allows a numerical

evaluation of weight fractions of alloying elements in the weld pool and weld metal, based on information on the chemical composition of the used welding consumables.

Algorithm of calculation of the concentrations on the moving interface. Applying the approach outlined in [7], we will believe that on the interface of the nonmetallic inclusion and liquid steel the reaction runs by the following equation:

$$xM + yQ = M_x Q_y, \tag{7}$$

where M is the metal (alloying) element (Al, Mn, Ti, Si, etc.), Q is the nonmetal element (O, N, S, etc.).

For such a reaction the equilibrium constant is given by the following equation:

$$k_{\text{eq}} = \frac{a_{M_x Q_y}}{a_M^x a_Q^y} = \frac{1}{\left[f_M c_M^i \right]^x \left[f_Q c_Q^i \right]^y} = \exp\left(-\frac{\Delta G^0}{RT} \right), \tag{8}$$

where $a_{M_x Q_y}$, a_M, a_Q are the activities of substances $M_x Q_y$, M; Q, c_Q^i are the concentrations on M and Q interphase, respectively, wt.%; f_M, f_Q are the coefficients of activity of M and Q, respectively; ΔG^0 is the standard free energy of exchange for reaction (7).

Considering the ratio of M and Q flows on the interface of the growing inclusion, the following equation can be derived:

$$c_M^i = c_M^b - \frac{xm}{ym_Q} \sqrt{\frac{}{D_M}} \left(c_Q^b - c_Q^i \right) \tag{9}$$

where c_M^b, c_Q^b are the concentrations of M and Q (wt.%) in the metal depth; m_M, m_Q are the atomic masses of M and Q; D_M, D_Q are the atomic masses of M and Q in the liquid steel.

Then, the interphase concentrations of M and Q, i.e. c_M^i, c_Q^i can be found by solving equations (8) and (9).

Considering the special structure of equations of this system, we obtained the following equation for the sought value of oxygen concentration c_Q^i on the interface

$$c_Q^i = \left(c_Q^i \right)^{-y/x} \frac{1}{P \sqrt[x]{k_{\text{eq}}}\, f_M f_Q^{y/x}} - \frac{c_M^b}{P} + c_Q^b, \tag{10}$$

where for brevity we denote:

$$P = (x/y)\left(m_M / m_Q \right) \sqrt{D_Q / D_M}.$$

We will solve equation (10) approximately by bitwise division method with the number of digits 10, providing the number of decimal places, corresponding to the order of the specified accuracy of the solution.

Finding c_Q^i for the *i-th* element, we numerically determine the value of concentration of the alloying element on the interface by equation (9).

Algorithm for evaluation of average density of nonmetallic inclusion. In condition (4) the current value of nonmetallic inclusion density, depending on the process time, appears on the moving interphase. Used as the estimate of the above density, was average density of the nonmetallic inclusion, determined from those considerations that the ratio between the quantity of oxides in the nonmetallic inclusion at each moment of time is numerically the same, as that in the equilibrium state of the oxide phase for the given temperature. It is rational to calculate the quantitative composition of the oxide phase by the slag theory, as that of a system with a collective electron phase, which in practically important cases is supported by the required set of numerical parameters [8].

In what follows, we shall number the values relating to elements and respective oxides by i index, for brevity.

Having denoted as $C_i (i = 1, n)$, C_0 the concentrations of i-th element-deoxidizer and oxygen, respectively; their coefficients of activity as $f_i (i = 1, n)$, f_0; coefficients of activity of oxides in molten slag relative to standard state of pure oxides as γ_i, we determine equilibrium constants K_i of reactions (6) of i-th oxide formation by the following formula:

$$K_i = \frac{x_i \gamma_i}{C_i^m C_0^n f_i^m f_0^n}, \tag{11}$$

where x_i are the mole fractions of the oxide phase components.

Set of relations (11) is a system of equations with respect to the molar fractions of the oxide phase components. Solving this system, taking into account the calculated coefficients of activities, we obtain the refined content of oxygen in steel and the respective composition of the slag phase, formed at certain equilibrium conditions.

Calculated composition of the oxide phase is equal to, (wt.%):

$$X_i(\%) = \frac{x_i M_i}{\sum_{i=1}^{n} x_i M_i},$$

where index i denotes the following oxides of elements in slag: FeO, MnO, SiO_2, Al_2O_3, TiO, etc.; M_i is the molecular mass of the respective oxide.

Algorithm of numerical realization of problem (1)–(6) and calculated model. The main difficulty when solving problem (1)–(6) is the need to allow for boundary condition (4) on the moving interface. Used for this purpose was the grid method from the numerical solution of this type of problems in the so-called variant of «catching» the unknown melt-inclusion interphase in the discrete grid node, earlier used in [4] for a problem with one diffusion equation.

As in mathematical model (1)–(6) the diffusion equations in the system are connected only through the condition on the moving interphase (4), the mentioned condition can be used for iterative refining of the step in time, that allows considering diffusion equations (1) in each time step as independent ones.

In order to solve the defined problem by the difference method, we will form grid ω, uniform along radial coordinate *r*, with constant step *h*, which at each moment of time $t = t_k$ consists of a plurality of points.

$$\omega^{(k)} = \left\{ r_i^{(k)} = a\left(t_k\right) + ih,\ i = \overline{0, M} \right\}.$$

Let moment of time τ_k be such that during time from t_k to $t_{k+1} = t_k + \tau_k$ inclusion radius changes by the value of grid step *h*, so that $a(t_{k+1}) - a(t_k) = h$. Then plurality of grid nodes at moment of time $t = t_{k+1}$ will be described by the following equation

$$\omega^{(k+1)} = \left\{ r_i^{(k+1)} = r_{i+1}^{(k)},\ i = \overline{0, M-1} \right\}.$$

Denoting the content of an arbitrary melt component by $C_n = C_n(r, t)$ and using standard designations, we will write a discrete equation, approximating the respective differential equation in system (1) on grid $\omega^{(k+1)}$, in the following form

$$\frac{C_{n,i}^{(k+1)} - C_{n,i+1}^{(k)}}{\tau_k} = \frac{1}{\left(r_i^{(k+1)}\right)^2 h} \times$$

$$\times \left[d_{n,i+1/2}^{(k+1)} \left(r_i^{(k+1)} + \frac{h}{2} \right)^2 \frac{C_{n,i+1}^{(k+1)} - C_{n,i}^{(k+1)}}{h} - \right. \qquad (12)$$

$$\left. - d_{n,i-1/2}^{(k+1)} \left(r_i^{(k+1)} - \frac{h}{2} \right)^2 \frac{C_{n,i+1}^{(k+1)} - C_{n,i}^{(k+1)}}{h} \right], i = \overline{1, M-2},$$

where

$$C_{n,i}^{(k+1)} = C_n\left(r_i^{(k+1)}, t_{k+1}\right),$$

$$C_{n,i}^{(k)} = C_n\left(r_i^{(k)}, t_k\right),\ d_{n,i\pm1/2}^{(k+1)} = D_n\left(T\left(t_k \pm \frac{\tau_k}{2}\right)\right).$$

Difference analogs of boundary conditions (2) and (5) have the following form

$$C_{n,0}^{(k+1)} = C_{n,0}^{(k)}; \qquad (13)$$

$$C_{n,M-1}^{(k+1)} = C_{n,M-2}^{(k)}. \qquad (14)$$

Value of time step τ_k, during which inclusion boundary moves per one node of the grid is obtained as the limit of time iterations $\tau_k^{(0)}, \tau_k^{(1)}, \tau_k^{(2)}, \ldots, \tau_k^{(s)}$. The above iteration process for refining the time step for transition from the *k*-th to (*k*+1)-th time layer was realized as follows:

1) the value of time step in the previous layer, i.e. $\tau_k^{(0)} = \tau_{k-1}$ was used as the initial approximation for τ_k;

2) having $\tau_k^{(s)}$ values, we solve by the method of sweeping *N* systems of linear difference equations of (12)–(14) form with $\tau_k = \tau_k^{(s)}$ for $n = \overline{1, N}$ and thus determine $C_{n,i}^{(k+1)}$ values. Note that here the following quantity X_n of *n*-th component of the melt will be transported to inclusion surface during time $\tau_k^{(s)}$:

$$X_n = 4\pi a^2\left(t_{k+1}\right) M_n d_{n,1/2}^{(k+1)} \frac{C_{n,1}^{(k+1)} - C_{n,0}^{(k+1)}}{h} \tau_k^{(s)};$$

3) we solve problem (9)–(10) for calculation of equilibrium concentrations of metal elements on boundary $a(t_{k+1})$;

4) proceeding from the found equilibrium composition, we calculate the average inclusion density $\rho_{k+1}^{(s)}$ and mass $m^{(s)}$ of the substance which precipitated into a layer of thickness $h^{(s)}$;

5) if the condition of completion of iteration process is true

$$\left| 1 - \tau_k^{(s)} \Big/ \tau_k^{(s-1)} \right| < \varepsilon,$$

for sufficiently small values ε (for instance, $\varepsilon = 10^{-4}$), then we assume time step value $\tau_k = \tau_k^{(s)}$ and go over to the next time layer; if this condition is not fulfilled, we find the next approximation $\tau_k^{(s+1)}$ for the time layer from the following relationship

$$4\pi\rho_{k+1}^{(s)} \left[a^3\left(t_{k+1}\right) - a^3\left(t_k\right) \right] \Big/ 3\tau_k^{(s+1)} = m^{(s)} \Big/ \tau_k^{(s)},$$

which is the difference analog of condition (6);

6) in equality (11) we establish $C_{n,0}^{(k+1)} = C_{n,\text{eq}}^{(s)}$ and go back to item 2).

Example of computation results. Computer realization of the developed calculation model was performed using Visual C^{++} programming system.

Figures 1, 2 give graphic illustrations of the respective computations by the developed computer program for one of the 20 studied variants of the metal of welds deposited by arc welding process using experimental fluxes, in keeping with the requirements of DSTU ISO 6847 standard [10].

Complete description of the conditions of performance of comparative analysis, as well as computation and experimental results requires separate consideration in the next publication.

The following values were used as input parameters during numerical estimation of initial content of alloying elements in the weld pool:

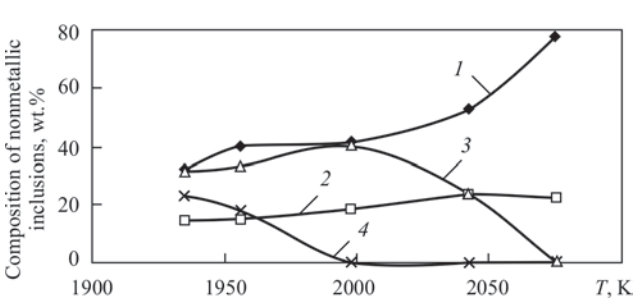

Figure 1. Change of the composition of nonmetallic inclusions at cooling of the weld pool: *1* – Al_2O_3; *2* – TiO_2; *3* – MnO; *4* – SiO_2

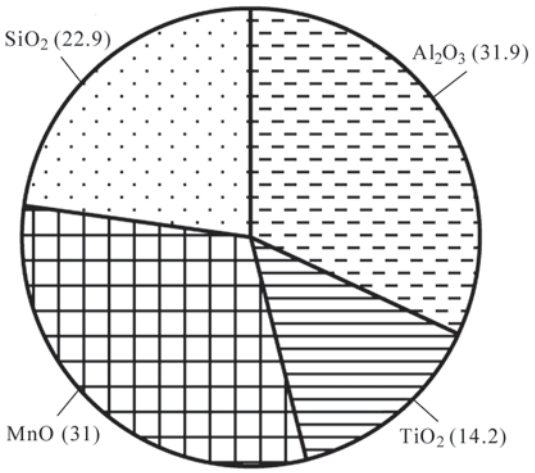

Figure 2. Results of calculation of final composition of nonmetallic inclusions in the deposited metal, wt.%

● flux composition, represented in the oxide layer; it was assumed that the initial composition of the slag system coincides with that of flux and contains the following (all or some of those listed below) components: SiO_2 = 40 %, Al_2O_3 = 40 %, CaF_2 = 20 %, MgO = 0 %, MnO = 0 %, TiO_2 = 0 %, CaO = 0 %, the sum of percentages of which should be equal to 100 %;

● alloying element content in steel, wt.%: 0.88 Si, 0.001 Ti, 0.64 Mn; 0.02 Al;

● alloying element content in welding wire, wt.%: 0.065 Si, 0.01 Ti, 0.98 Mn, 0.002 Al;

● oxygen content, wt.%: 0.02 in steel and 0 in the wire;

● relative fraction (0.33) of base metal in weld pool metal;

● temperature characteristics of the modeled process were calculated by the procedure of N.N. Rykalin.

Conclusions

A mathematical model of the considered process was developed on the basis of physico-chemical description of formation of endogenous nonmetallic multicomponent inclusions in the weld metal. The mathematical model allows for the kinetics and heterogeneity of the process, in particular, the nonstationary diffusion transfer of reagents (specifically, deoxidizer-elements) to the inclusion surface and reaction on melt-inclusion interface, as well as presence of a two-phase zone during weld solidification. The mathematical model is a nonstandard nonlinear boundary problem for a system of diffusion equations with the specific condition on a moving interface.

The mathematical model was the basis for development of a calculation model, which envisages thermodynamic calculation of the local equilibrium state on the moving interface and numerical solution of the boundary problem for a system of differential equations of parabolic type based on discretization, using the grid method in the variant of catching the moving boundary into the grid node.

Developed respective computer program can be used for numerical prediction in a computational experiment of the size and composition of oxide (after some modification also oxysulphide) nonmetallic inclusions, depending on the concentration and thermal conditions in the weld pool.

1. Gubenko, S.I., Parusov, V.V., Derevyanchenko, I.V. (2005) *Nonmetallic inclusions in steel*. Dnepr, ART-PRESS [in Russian].
2. Ozhigov, L.S., Mitrofanov, A.S., Rybalchenko, N.D. et al. (2017) Influence of nonmetallic inclusions in low-alloy carbon steel on service life of NPP piping. *Voprosy Atomnoj Nauki i Tekhniki*, 110 (**4**), 59–64 [in Russian].
3. Myasnikova, A.A. (2012) Nonmetallic inclusions and their influence on welded joint quality in manual arc welding. *Master's J.*, **1**, 50–54.
4. Hong, T., Debroy, T., Babu, S.S., David, S.A. (2000) Modeling of inclusion growth and dissolution in the weld pool. *Metallurg. and Mater. Transact. B, 31B*, **1**, 161–169.
5. *Kwon* Yu-Jong, Zhang Jian, Lee Hae-Geon (2008) A CFD-based nucleation-growth-removal model for inclusion behavior in a gas-agitated ladle during molten steel deoxidation. *ISIJ Int.*, 48(**7**), 891–900.
6. Golovko, V.V., Taraborkin, L.A. (2016) Modelling of chemical composition of weld pool metal in arc methods of welding. *The Paton Welding J.*, **1**, 12–16.
7. Hong, T., Debroy, T. (2001) Time-temperature-transformation diagrams for the growth and dissolution of inclusions in liquid steels. *Scripta Materialia*, 44(**5**), 847–852.
8. Grigoryan, V.A., Stomakhin, A.Ya.. Ponomarenko, A.G. et al. (1989) *Physical-chemical calculations of electric steelmaking processes*. Moscow, Metallurgiya [in Russian].
9. Pokhodnya, I.K., Demchenko, V.F., Demchenko, L.I. (1979) *Mathematical modeling of gas behavior in welds*. Kiev, Naukova Dumka [in Russian].
10. *DSTU ISO 6847:2015 (ISO 6847:2013, IDT)*: Welding consumables. Deposition of a weld metal pad for chemical analysis [in Ukrainian].

Received 18.12.2018

DOI: http://dx.doi.org/10.15407/tpwj2018.02.02

EFFECT OF METAL STRUCTURE ON SERVICE PROPERTIES OF HIGH-STRENGTH STEEL WELDED JOINTS PRODUCED USING DIFFERENT METHODS OF WELDING*

L.I. MARKASHOVA, V.D. POZNYAKOV, V.D. SHELYAGIN, E.N. BERDNIKOVA, A.V. BERNATSKY and **T.A. ALEKSEENKO**
E.O. Paton Electric Welding Institute of the NAS of Ukraine
11 Kazimir Malevich Str., 03150, Kyiv, Ukraine. E-mail: office@paton.kiev.ua

Evaluations of effect of forming structures and phase constituents on change of the most significant mechanical properties of welded joints were carried out based on investigation of peculiarities of formation of structural parameters in welded joints of high-strength steel, produced by different methods of fusion welding (laser, arc and hybrid laser-arc). A role of structural factors (alloying, phase constituents, grain, subgrain structure, distribution and density of dislocations, phase precipitations, their size and nature of distribution) was shown in providing the optimum properties of the welded joints and their service reliability. It is shown that the most significant structural-phase parameters and factors, providing under operation conditions, the necessary complex of properties of welded joints, namely strength (σ_y), fracture toughness (K_{1C}) and crack resistance (τ_{in}), are fineness of grain and subgrain structures; dispersion of phase precipitations at their uniform distribution; absence of extended dislocation accumulations — potential concentrators of internal stresses (zone of nucleation and propagation of cracks). 23 Ref., 6 Figures.

Keywords: *laser welding, arc welding, hybrid laser-arc welding, high-strength steel, welded joints, structure, phase composition, mechanical properties, fracture toughness, crack resistance*

High-strength steels with 700 MPa yield point and more are widely used in the world practice in manufacture of metal structures of heavy-loaded machines and mechanisms. As a rule, welded joints, produced of such steels, have good resistance to static and dynamic loadings at positive as well as negative temperatures [1–5].

Manufacture of welded structures of high-strength steels is mostly carried out using mechanized or automatic welding in shielding gases, mainly it is a mixture based on argon with addition of 18–22 % of carbon dioxide. Rarely, automatic submerged-arc welding is used for these purposes. Manual arc welding with coated electrodes is still widely used in repair and assembly of structures from high-strength steels.

As a rule, solid and flux-cored wires of small diameter (1.2–1.4 mm) are used for mechanized gas-shielded welding as well as limitations of welding modes (I_w = 160–220 A, U_a = 21–28 V; v_w = 12–25 m/h). Under such welding conditions a cooling rate of HAZ metal of welded joints ($w_{6/5}$) in a temperature interval of the smallest austenite stability (for high-strength steels this makes 600–500 °C) can vary in a wide limits from 10 to 40 ° C/s. This allows providing required strength, ductility and impact toughness to the weld metal of high-strength steel welded joints including at negative temperatures.

The main disadvantage of indicate welding process lies in its low efficiency. Therefore, in recent time, it is an active search of new, more efficient processes applicable to high-strength steel welding. Laser and hybrid laser-arc welding can be referred to such processes. In comparison with arc welding these processes allow rising welding efficiency several times [6–8]. It is achieved due to increase of power of laser radiation source as well as rise of rate of its movement along the joint to 50–110 m/h.

However, as it is known [9–11], change of the technological modes of welding can result in significant changes of structure of weld metal and HAZ of welded joints and, respectively, to variation of their mechanical properties. These problems are poorly studied in scope of high-strength steels.

In this connection, the aim of presented work was investigation of effect of structure and phase com-

*Based on materials presented at VIII International Conference «Beam Technologies in Welding and Materials Processing», September 10–16, 2017, Odessa, Ukraine.
A.V. Siora and E.V. Polovetsky participated in the work.

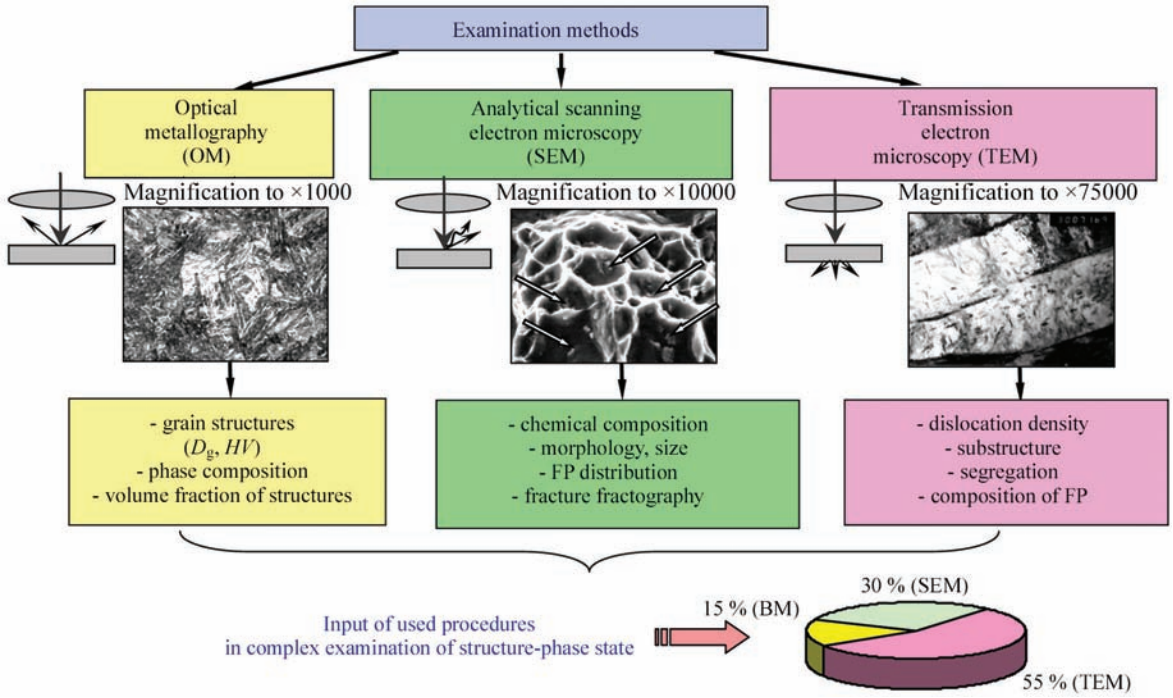

Figure 1. Block diagram of complex methods of examination

position of metal in a welding zone of high-strength steel joints produced by different welding methods (arc, hybrid, laser-arc, laser) on change of the most significant service properties of the welded joints.

To solve stated problems the investigations were carried out at all structural levels (using the methods of optical metallography, scanning and transmission electron microscopy) as for change of structure-phase state as well as dislocation density in different zones of welded joints, at different welding modes. Based on performed experimental investigations it was an analytical estimation of a role of structure-phase changes in the joint metal in formation of the most significant service properties of the welded joints, namely strength (σ_y), fracture toughness (K_{1C}) as well as crack resistance, caused by level of local internal stresses (τ_{in}) taking into account distribution of dislocation density (ρ).

Materials and investigation procedures. The investigations were carried out on the samples of 14KhGN2MDAFB high-strength steel (wt.% 0.183 C; 1.19 Cr; 0.98 Mn; 2.07 Ni; 0.22 Mo; 0.08 V; 0.33 Si; not more than 0.018 P and 0.005 S) of up to 10 mm thickness. In the case of arc and hybrid laser-arc welding Sv-10KhN2GSMFTYu solid section wire (wt.% ≤ 0.1 C; 0.7 Cr; 0.4 Mn; 0.22 Mo; 0.15 V; 0.24 Si; 0.007 S) was used. Laser welding was carried out without filler materials. The welded joints were produced at the following welding modes.

Arc welding. Welding was carried out in a rigid circuit at the next welding rates: 1st mode — v_w = 18 m/h; 2nd mode — 30 m/h; 3rd mode — 40 m/h; 4th mode — 50 m/h. Cooling rate of HAZ metal in 600–500 °C temperature interval made, respectively: $w_{6/5}$ ≈ 10–12; 19–22; 25–28; 38 °C/s; I_w = 220–240 A; U_a = 30–32 V.

Hybrid laser-arc welding: 1st mode — v_w = 72 m/h, I_w ~ 125 A, U_a ~ 23 V; 2nd mode — v_w = 90 m/h, I_w ~ ~ 150 A, U_a ~ 25 V; 3rd mode — v_w = 110 m/h, I_w ~ ~ 200 A, U_a ~ 26 V. Given modes provide cooling of HAZ metal in 600–500 °C temperature interval with $w_{6/5}$ ≈ 58–62 °C/s rate. Nd:YAG laser DY 044 (Rofin

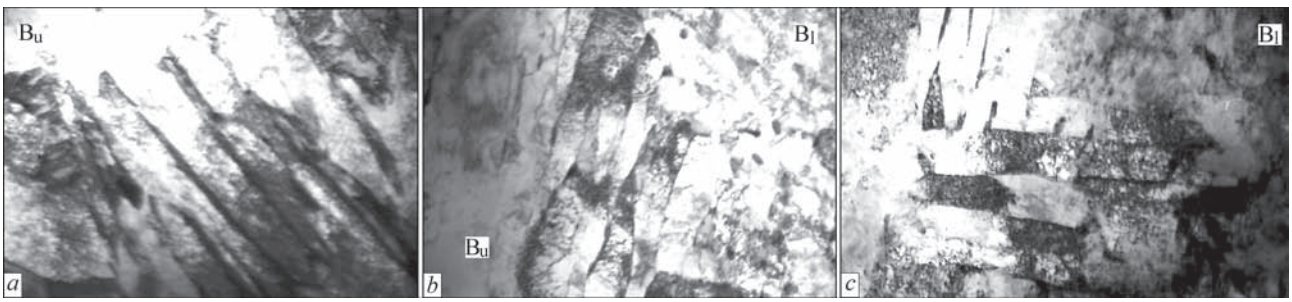

Figure 2. Fine structure (×30000) of weld metal of joints under conditions of different welding modes: *a* — arc; *b* — hybrid laser-arc; *c* — laser

Synar, Germany) of up to 4.4 kW power was used as a laser radiation source and shielding gas (Ar + CO_2 mixture with 15–20 l/min consumption).

Laser welding. Welded joints were received under conditions of different welding rates, i.e. 1st mode — v_w = 18 m/h; 2nd mode — v_w = 30 m/h; 3rd mode — v_w = 50 m/h and cooling rates of HAZ metal: $w_{6/5} \approx 28$; 50; 103 °C/s, respectively.

Methods of structure examinations. The examinations of structure-phase and concentration changes of chemical elements, nature of distribution and density of defects of crystalline lattice in weld metal and HAZ of the welded joints were studied using a complex of experimental methods of modern physical metallurgy, including optical metallography (microscopes «Versamet-2» and «Neophot-32»), analytical scanning electron microscopy (SEM-515, PHILIPS Company, Netherlands) and transmission electron microscopy (JEM-200CX, JEOL Company, Japan) (Figure 1). Hardness was measured on microhardness gage of LECO Company at 0.1 kg loading.

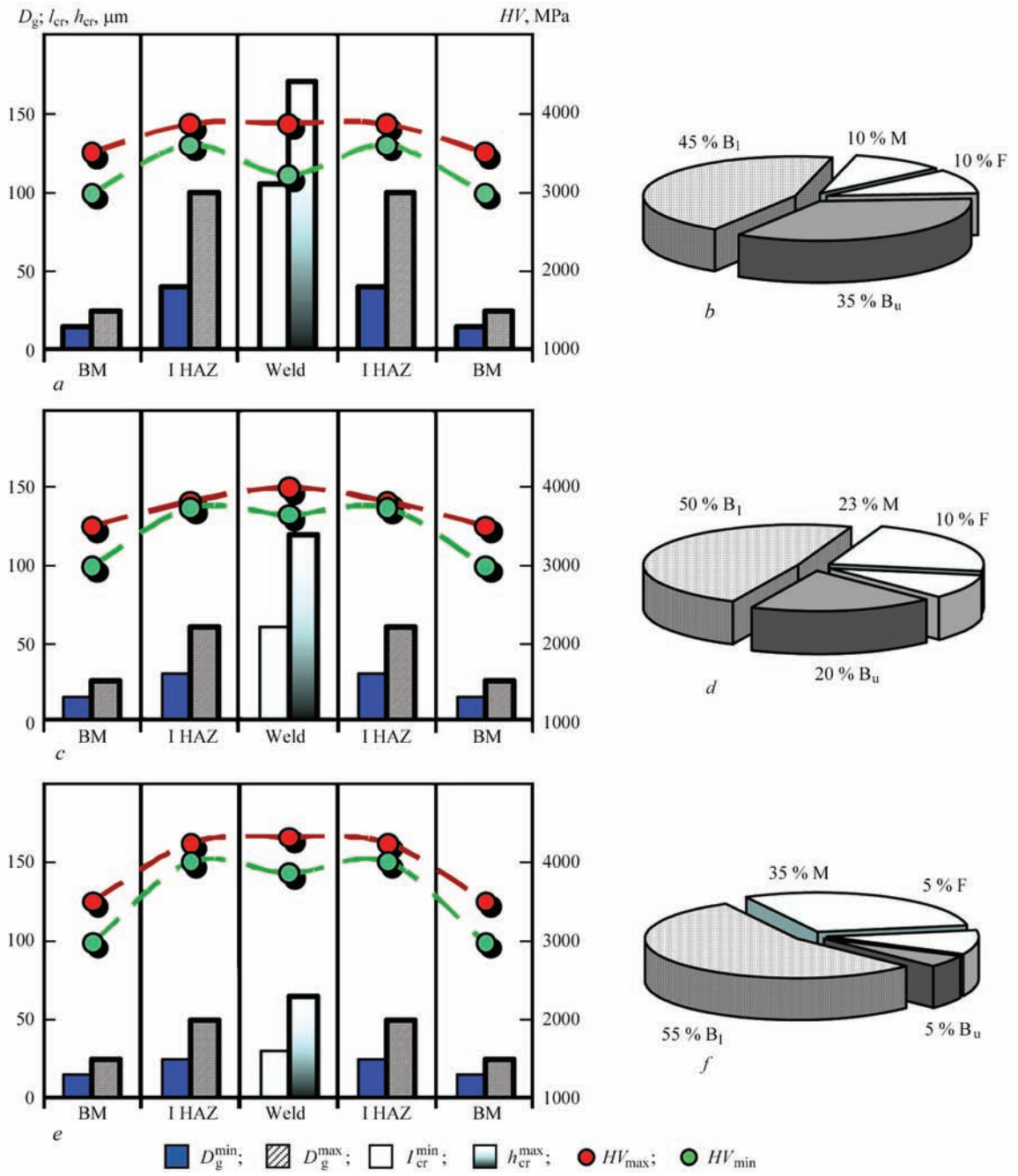

Figure 3. Change of structure parameters of forming phase constituents (B_l, B_u, F, M) at different modes of welding (*a*, *b* — arc, v_w = = 40 m/h; *c*, *d* — hybrid laser-arc, v_w = 72 m/h; *e*, *f* — laser, v_w = 50 m/h): *a*, *c*, *e* — change of grain size (D_g), width (h_{cr}) and length (l_{cr}) of crystallines, microhardness (*HV*) in base metal (BM), in weld metal (WELD), areas of coarse grain (I HAZ); *b*, *d*, *f* — volume fraction (%) of phase constituents

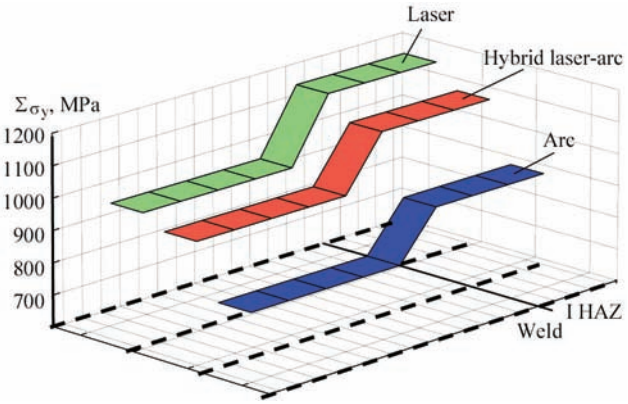

Figure 4. Change of average calculation value $\Sigma\sigma_y$ on zones of welded joints (I HAZ) (weld, I HAZ) of 14KhGN2MDAFB steel at different welding modes

Results of examinations. Changes of structure-phase composition in a welded material zone (steel 14KhGN2MDAFB) depending on welding modes are presented in Figures 2 and 3. Thus, in the case of arc welding (v_w = 18–50 m/h) formation of a structural state of the following type is observed in the weld metal, i.e. up to 45–65 % of upper bainite (B_u); 5–10 % of martensite (M); 10–20 % of ferrite (F) and 10–35 % of lower bainite (B_l). At transfer to overheating area (I HAZ) the next changes of structure types and their volume fraction are observed, namely B_u 20–45 %; M 15–20 %; F 5 % and B_l 30–45 % with typical structure of base metal of bainite-ferrite type. At that, in the case of v_w = 18 m/h the extended dislocation accumulations up to $\rho = (1–2)\cdot10^{11}$ cm^{-2} are formed in the weld metal along grain boundaries, mainly on B_u boundaries. It creates a high gradient of dislocation density (Figure 2, *a*) in such elements of the structure. Such structural changes can result in nonuniform level of mechanical properties along the welding zone and reduction of crack resistance of the welded joints.

Thus, the most significant (from point of view of crack resistance decrease) structural-phase changes (coarse grain gradient structure of mainly B_u) are typical for the welded joints produced using arc welding modes at v_w = 18 m/h.

The examinations of structure and phase composition of welded joints of 14KhGN2MDAFB steel in hybrid laser-arc welding showed that at transfer from v_w = 72 to 110 m/h phase composition of weld metal and HAZ overheating area is preserved the same (bainite-martensite), however, there is a noticeable reduction of B_l volume fraction (to 10–20 %). Transfer to v_w = 110 m/h promotes increase of the integral value of dislocation density to $\rho = 1.5\cdot10^{11}$ cm^{-2} and formation of mainly B_u structure.

The most uniform distribution of dislocation density ($\rho = (4–6)\cdot10^{10}$ cm^{-2}) is typical for structures of B_l at v_w = 72 m/h (Figure 2, *b*; Figure 3, *c*, *d*).

In the case of laser welding the examinations showed that increase of welding rate from v_w = 18 to 50 m/h causes change of phase composition of the weld metal from bainite-ferrite to bainite-martensite (Figure 3, *e*, *f*). At the same time, it should be emphasized that there is formation of mainly fine grain equiaxial B_l structure under conditions of uniform redistribution of volumetric dislocation density ($\rho = (8–9)\cdot10^{10}$ cm^{-2}), Figure 2, *b*.

In such a way, the examinations showed change of a relationship of forming in the welding zones phase constituents (B_l, B_u, M), their parameters, volume fraction as well as density and distribution of dislocations under conditions of variation of welding modes (from arc to hybrid and laser). Thus, under conditions of arc welding there is mainly formation of B_u structure at total increase of sizes of grain and subgrain structures with nonuniform distribution of dislocation density. Transfer to modes of hybrid, laser-arc and laser welding promotes mainly formation of B_l structures at significant refinement of grain

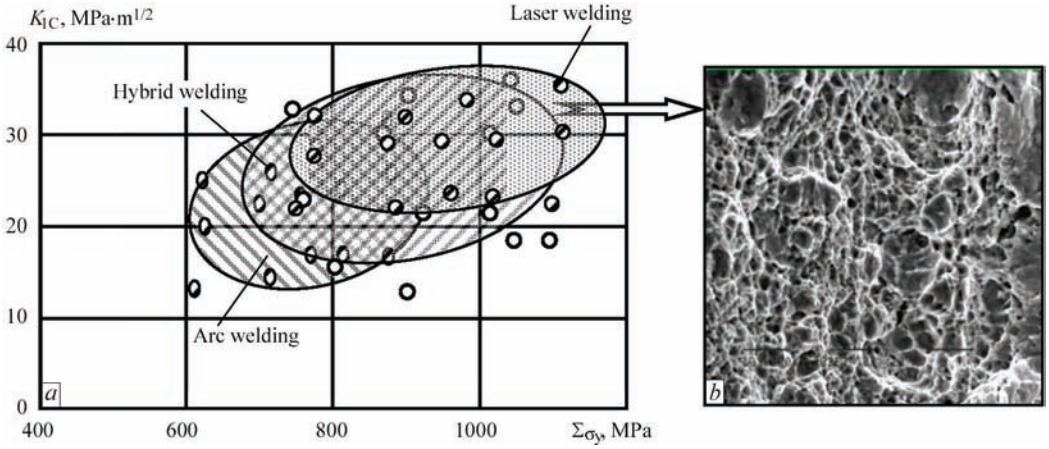

Figure 5. Change of calculation values of strength $\Sigma\sigma_y$ and toughness K_{1C}, (*a*) of metal of welds in arc, hybrid laser-arc, laser welding and fractogram (*b*) of tough fracture of welded joint, produced by laser welding (×2020)

and subgrain with uniform distribution of volume and grain-boundary dislocation density.

Analytical estimations of welded joint service properties. Following the examination of structure-phase changes at different modes of welding the analytical estimations of the most significant service properties of welded joints, namely indices of strength, toughness and crack resistance [12–18] were carried out.

The analytical estimations of strengthening $\Sigma\sigma_y$ were carried out according to known dependencies of Hall–Petch, Orowan, etc. [14–19]: $\Sigma\sigma_y = \Delta\sigma_0 + \Delta\sigma_{s.s} + \Delta\sigma_g + \Delta\sigma_s + \Delta\sigma_d + \Delta\sigma_{d.s}$, where σ_0 is the resistance of type of metal lattice to movement of free dislocations (stress of lattice friction or Peierls–Nabarro stress); $\sigma_{s.s}$ is the strengthening of solid solution by alloying elements (Mott–Nabarro dependence); σ_g, σ_s is the strengthening due to change of grain and subgrain value (Hall–Petch dependence); σ_d is the dislocation strengthening, caused by interdislocation interaction on theory of J. Taylor, A. Zager, N. Mott and G. Hirsch; $\sigma_{d.s}$ is the dispersion strengthening due to dispersion phase constituents by Orowan.

Calculation values of fracture toughness indices K_{1C} were estimated on Krafft dependence [20] K_{1C} =

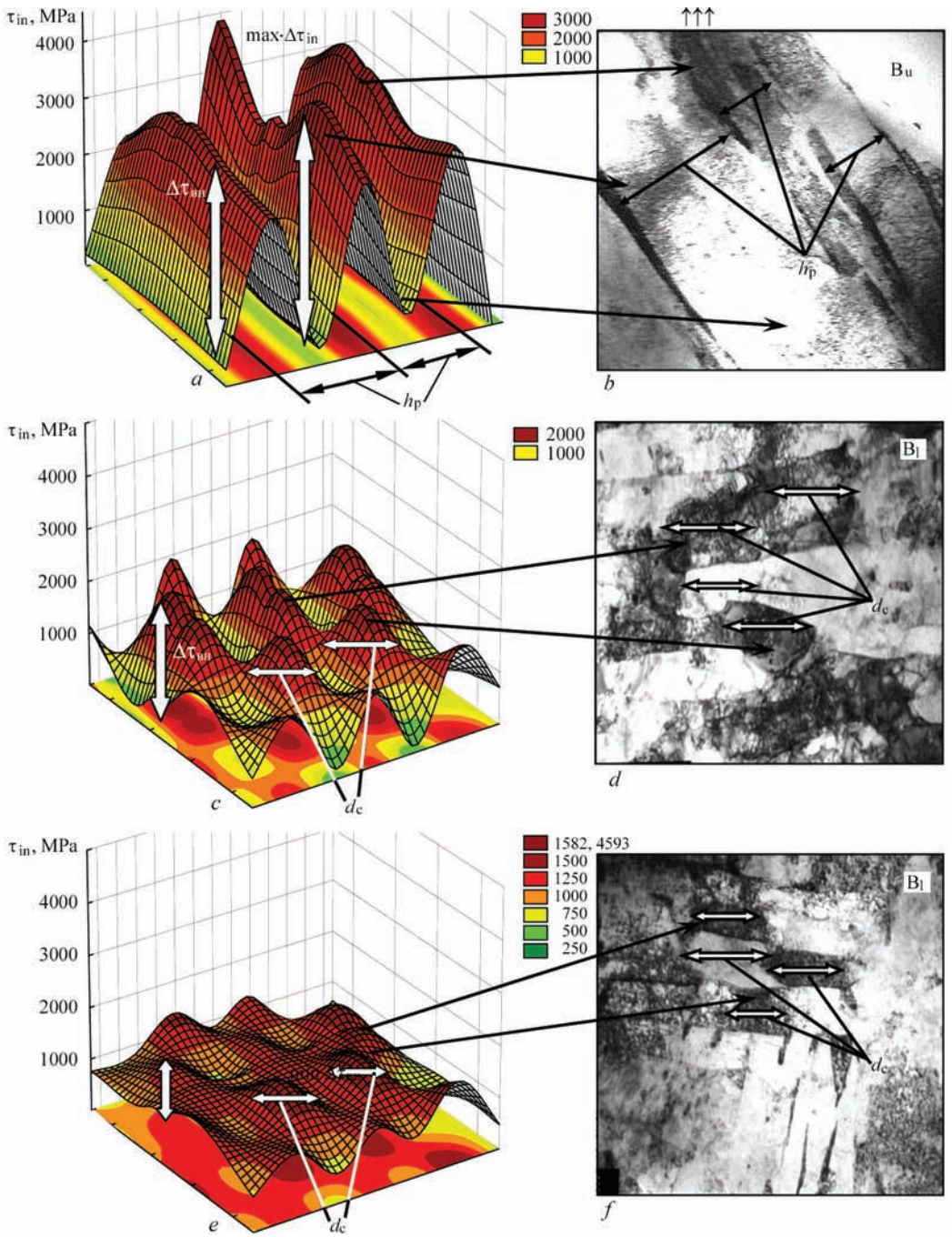

Figure 6. Distribution of local internal stresses (τ_{in}) in metal of welded joints in structural zones: *a*, *b* — B_u in arc welding; *c*, *d* — B_l in hybrid laser-arc; *e*, *f* — B_l in laser welding (*b*, *d*, *f*, ×30000)

$= (2E\sigma_{d.s}\delta_c)^{1/2}$, where E is the Young's modulus; σ_y is the calculation value of strengthening; δ_c is the value of critical opening of crack (according to data of substructure parameters).

Following the analysis of approaches to mechanisms of crack nucleation and material fracture the estimation based on dislocation theory of crystalline solids was selected taking into account nature of dislocation structure and its distribution (dislocation accumulations or uniform distribution of dislocations) [21–23]. A field of internal stresses, developed by dislocation structure (dislocation density) is determined by $\tau_{in} = Gbh\rho/[\pi(1 - \nu)]$ dependence, where G is the shear modulus; b is the Burgers vector; h is the foil thickness; ν is the Poisson's ratio; ρ is the dislocation density [22].

The next was determined as a result of carried estimations. Under conditions of arc welding (v_w = = 40 m/h) the calculation value of $\Sigma\sigma_y$ = 741–890 MPa (Figure 4) in the weld metal and HAZ, respectively. At that fracture toughness index K_{1C} makes around 12–35 MPa·m$^{1/2}$ (Figure 5). Under conditions of modes of hybrid laser-arc (v_w = 72 m/h) and laser welding (v_w = 50 m/h) $\Sigma\sigma_y$ = 850–1080 MPa and $\Sigma\sigma_y$ = 900–1120 MPa, respectively, at increase (by 10–20 %) of level of fracture toughness (Figure 5). The latter is caused by preferable formation of B_l structure at uniform distribution of dislocation density ρ and absence of areas of brittle cleavage on the fracture surface of welded joints (Figure 5, *b*).

The calculation estimations of local internal stresses τ_{in}, given on diagrams of Figure 6, show the following.

The extended zones with maximum values of τ_{in} (1900–3700 MPa) are formed under conditions of arc welding (18 m/h) along grain boundaries of B_u in the places of extended dislocation accumulations (ρ = = (1–2)·10^{11} cm^{-2}), Figure 6, *a*, *b*. This results in nucleation of microcracks in these zones and decrease of crack resistance of welded joints. Reduction of τ_{in} is typical for welded joints produced on hybrid welding modes τ_{in} = 1470–1867 MPa, $\rho = 8\cdot10^{10}$–$1\cdot10^{11}$ cm^{-2} (Figure 6, *c*, *d*) at v_w = 72 m/h and particularly on modes of laser welding τ_{in} = 1470–1663 MPa, ρ = = (8–9)·10^{10} см$^{-2}$ (Figure 6, *e*, *f*), that promotes formation in a welding zone of fine grain and fragmented B_l structures in combination with uniform distribution of dropping dislocation density.

As a result it is determined that the optimum properties of strength, toughness and crack resistance in high-strength steel welded joints are provided under conditions of laser welding (v_w = 50 m/h) that is caused by formation of more dispersed structures, i.e. B_l, fine grain tempered M at absence of extended dislocation accumulations, namely stress concentrators of local internal stresses $\tau_{in.}$

Conclusions

1. Investigations were carried out on structure and service properties of welded joints of 14KhGN2MDAFB high-strength steel depending on used modes of welding (arc, hybrid laser-arc and laser).

2. It is shown that the following transformations of structure are observed under different conditions of welding of 14KhGN2MDAFB steel, namely change of relationship of phase constituents (B_l, B_u, M) forming in the welding zones as well as their parameters and volume fraction. B_u structures are mainly formed under conditions of arc welding at general increase of size of grain and subgrain structures with their non-uniform distribution and gradient dislocation density.

3. Transfer to modes of hybrid laser-arc and laser welding promotes formation of B_l structures with sharp refinement of grain and subgrain structure at uniform distribution of dislocation density.

4. Analysis of interaction: welding modes → structure → properties indicates significant increase of service properties (strength, fracture toughness, crack resistance) of welded joints of 14KhGN2MDAFB high-strength steel at transfer to laser welding modes, that is related with prevailing effect of fine granulation of forming B_l structures, absence of dense extended dislocation accumulations with preferably uniform distribution of dislocations in the welding zone.

1. (1965) *High-strength steel:* Transact. Ed. by L.K. Gordienko. Moscow, Metallurgiya [in Russian].
2. Houdremont, E. (1959) *Special steels*. Moscow, Metallurgizdat [in Russian].
3. Shorshorov, M.Kh., Belov, V.V. (1972) *Phase transformations and properties of steel in welding*. Moscow, Nauka [in Russian].
4. Madej, K., Jachym, R. (2017) Welding of high strength toughened structural steel S960QL. *Biuletyn Instytutu Spawalnictwa*, **2**, 6–16.
5. Rozanski, M., Stano, S., Grajcar, A. (2016) Effect of braze welding parameters on the structure and mechanical properties of joints made of steel CPW 800. Pt 1: Arc braze welding. *Ibid*., **6**, 6–12.
6. Cah, P., Salminen, A., Martikainen, J. (2010) Laser-arc hybrid welding processes (Review). *The Paton Welding J*., **6**, 32–40.
7. Kurc-Lisiecka, A., Lisiecki, A. (2017) Laser welding of the new grade of advanced high-strength steel DOMEX 960. *Materials and Technology*, 51(**7**), 199–204.
8. Liu, F., Yu, X., Huang, C. et al. (2015) Microstructure and mechanical properties of AerMet 100 ultra-high strength steel joints by laser welding. *J. of Wuhan Univ. of Technology — Mater. Sci. Ed*., 30(**4**), 827–830.

9. Keehan, E., Zachrisson, J., Karlsson, L. (2010) Influence of cooling rate on microstructure and properties of high strength steel weld metal. *Sci. and Technol. of Welding and Joining*, **15**, 233–238.
10. Svensson, L.-E. (2007) Microstructure and properties of high strength weld metals. *Mat. Sci. Forum*, **539–543**, 3937–3942.
11. Mikhoduj, L.I., Yushchenko, A.K., Poznyakov, V.D. et al. (1991) Weldability of high-strength steel 12GN3MFAYuDRSSh. *Avtomatich. Svarka*, **11**, 12–16 [in Russian].
12. Markashova, L.I., Poznyakov, V.D., Berdnikova, E.N. et al. (2016) Structure and service properties of hybrid laser-arc welded joints of 14KhGN2MDAFB steel. *The Paton Welding J.*, **5–6**,104–113.
13. Markashova, L.I., Poznyakov, V.D., Berdnikova, E.N. et al. (2014) Effect of structural factors on mechanical properties and crack resistance of welded joints of metals, alloys and composite materials. *Ibid*., **6–7**, 22–28.
14. Goldshtejn, M.I., Litvinov, V.S., Bronfin, B.M. (1986) *Metallophysics of high-strength alloys*. Moscow, Metallurgiya [in Russian].
15. Conrad, H. (1973) Model of strain strengthening for explanation of grain size effect on yielding of metal. *Ultrafine grain in metals*. Ed. by L.K. Gordienko. Moscow, Metallurgiya, 206–219 [in Russian].
16. Petch, N.J. (1953) The cleavage strength of polycrystalline. *J. Iron and Steel Inst*., **173**, 25–28.
17. Orowan, E. (1954) Dislocation in metals. New York, AIME.
18. Ashby, M.F. (1983) Mechanisms of deformation and fracture. *Adv. Appl. Mech.*, **23**, 117–177.
19. Busha, Yu., Karel, V., Longauer, C., Billy, I. (1977) About relation of yield strength of sorbite with medium size carbides. *Fizika Metallov i Metallovedenie*, 44(**3**), 604–610 [in Russian].
20. Romaniv, O.N. (1979) *Fracture toughness of structural steels*. Moscow, Metallurgiya [in Russian].
21. Stroh, A.N. (1954) The formation of cracks as a recoil of plastic flow. *Proc. of the Roy. Soc. A*, 223(**1154**), 404–415.
22. Panin, V.E., Likhachev, V.A., Grinyaeva, Yu.V. (1985) *Structural levels of deformation of solids*. Siberian Depart., Nauka [in Russian].
23. Conrad, H. (1963) Effect of grain size on the lower and flow stress of iron and steel. *Acta Metallurgica*, **11**, 75–77.

Received 04.12.2017

DOI: http://dx.doi.org/10.15407/tpwj2018.02.03

INFLUENCE OF CORROSION DAMAGE ON CYCLIC LIFE OF BUTT WELDED JOINTS STRENGTHENED BY HIGH-FREQUENCY MECHANICAL PEENING

V.V. KNYSH, S.A. SOLOVEJ, L.I. NYRKOVA and **V.N. MIRYANIN**
E.O. Paton Electric Welding Institute of the NAS of Ukraine
11 Kazimir Malevich Str., 03150, Kyiv, Ukraine. E-mail: office@paton.kiev.ua

In the article, the results of investigation of efficiency of applying the technology of high-frequency mechanical peening for increasing the fatigue resistance characteristics of butt welded joints of steel 15KhSND with a subsequent long-term effect of the environment climatic factors, characteristic for a moderate cold marine climate are given. The effect of given climate was modeled by holding the joints in the salt fog chamber KST-1 at the temperature of (35 ± 2) °C and during spraying the sodium chloride solution for 15 minutes every 45 minutes. The duration of corrosion tests of specimens in the chamber KST-1 was 1200 h. After holding in the chamber KST-1, the metallographic examinations of the surface layer of the weld metal and the metal of heat-affected zone of welded joints in the initial (non-strengthened) state and in the state strengthened by this technology were carried out. The depth and degree of damage by corrosion spots and cavities of surface layers of weld metal and heat-affected zones of welded joints were calculated. The fatigue resistance characteristics of welded joints in the initial (non-strengthened) state and in the state strengthened by high-frequency mechanical peening were experimentally established after effect of a neutral salt fog for 1200 h. 11 Ref., 1 Table, 6 Figures.

Keywords: *butt welded joint, neutral salt fog, fatigue, high-frequency mechanical peening, increase in resistance to corrosion fatigue*

Due to a high efficiency, the technology of high-frequency mechanical peening (HMP) is widely used not only to increase the fatigue resistance characteristics of welded joints at the stage of manufacturing the metal structures, but also in repair and restoration works [1–5]. In the world literature HMP technology has also received other names: ultrasonic impact treatment, ultrasonic peening, high-frequency mechanical impact treatment [1–11]. This is connected with the fact that to perform peening of welded joints at a high frequency of the striker impact against the treated surface, the ultrasonic power is used in the HMP equipment. In the articles of recent years, the calculation of effectiveness of applying HMP technology by numerical modeling is ever often found, depending on the condition of surface layer of the material, technological parameters of treatment, induced residual compressive stresses, etc. [6–8]. These calculation models assume that the metal surface layer, plastically deformed by HMP technology, remains unchanged during the entire designed service life. However, the majority of welded metal structures (bridges, cranes, hoisting-and-transport machines, railway transport, etc.) are subjected to simultaneous action of external alternating loading and corrosive-aggressive environments in the process of long-term operation. A long-term effect of corrosive media can lead to a partial or complete corrosion-mechanical loss of the strengthened metal layer, to decrease in the designed characteristics of fatigue resistance and, accordingly, to premature fracture of the structure [9, 10]. Thus, in the work [9], the characteristics of fatigue resistance of butt welded joints of rails in the initial state, after HMP and after HMP with the subsequent holding for 450 h in the synthetic sea water (105 g/l NaCl + 12.7 g/l $MgCl_2$ + 7.7 g/l $MgSO_4 \cdot 7H_2O$ + + 12.15 g/l $CaSO_4 \cdot 2H_2O$ + + 0.5 g/l $CaCO_3$) were investigated. It was established that the value of limited endurance on the base of $2 \cdot 10^5$ cycles of welded joints in the initial state was 256 MPa, after HMP — 314 MPa, and after HMP with the subsequent holding in the corrosive medium — 290 MPa. Despite the detailed description of structure of welded joints in the initial state and after HMP in this work, the causes for decrease in the value of limited endurance by 8 % on the base of $2 \cdot 10^5$ cycles after holding in the corrosive medium are not investigated. In the work [10] it was experimentally established that holding of T-welded joints of steel 15KhSND, strengthened by HMP, in the salt fog chamber KST-1 (at a temperature of (35 ± 2) °C and spraying a sodium chloride solution for 15 min every 45 min) leads to decrease in their value of limited endurance on the base of $2 \cdot 10^6$ cycles approximately by 24.5 % (from 265 to 200 MPa). This is caused by a significant fracture of the metal layer

strengthened by HMP (in some areas only traces of strengthened metal layer remained). Despite this, the value of limited endurance of joints, strengthened by HMP, based on $2 \cdot 10^6$ cycles is 48 % higher than that of the non-strengthened ones. The results of works [9, 10] show that investigation of regularities of fatigue resistance of welded joints, strengthened by HMP at a long-term holding in the corrosive media, and, correspondingly, at a certain damage of the plastically deformed metal layer, is an actual problem. The significant corrosion damages, characteristic to welded joints of metal structures, operated in the conditions of a moderately cold marine climate, as is shown in the work [10], can be obtained by preliminary holding of welded joints in the salt fog chamber.

The aim of the present work is to evaluate the effectiveness of applying HMP technology for increasing the fatigue resistance characteristics of welded joints of metal structures at the subsequent long-term exposure to environmental climatic factors, which are characteristic to the moderately cold marine climate.

Material and methods of investigations. The experimental investigations were carried out on specimens of butt welded joints of low-alloyed steel 15KhSND, which is widely applied for manufacture of elements of metal structures for long-term service (for example, in span structures of railway and road bridges), has an increased strength, good weldability, it is stable in the atmospheric conditions and serviceable in the temperature range from –70 to 45 °C. The chemical composition of the steel is, wt.%: 0.142 C; 0.466 Si; 0.63 Mn; 0.020 S; 0.013 P; 0.31 Ni; 0.66 Cr; 0.34 Cu. The mechanical properties are σ_y = = 400 MPa, σ_t = 565 MPa, δ_5 = 26 %.

The blanks for specimens of butt welded joints were cut from 12 mm thick hot-rolled sheet steel of 12 category in the direction of rolling. The size of blanks was 600×175 mm. The butt welded joints were produced by double-sided, single-arc automatic welding of plates without edge preparation (gap along the butt was 0–1.0 mm) under the flux of OP 192 (Oerlikon Company) using the wire Sv-08G1N-MA of 4 mm diameter. The welding was carried out at reverse polarity of the electric rectifier VSZh-1600. The welding modes of the first weld were: U = 55 V, I = 650–700 A, v = 26.7 m/h; and of the second weld (on the opposite side) were: U = 57 V, I = 760–780 A, v = 26.7 m/h. The second weld was produced only after the first weld was completely cooled. After welding, from each of the produced welded plates of 600×350 mm, 8 specimens of 350×70 mm were cut. The shape and geometric sizes of specimens of butt welded joints are shown in Figure 1.

The experimental investigations were carried out in the electro-hydraulic machine URS-20 at alternating tension with an asymmetry of the cycle R_σ = 0 and frequency of 5 Hz. The criterion for test completion was the complete fracture of specimens or the excess of testing base of $2 \cdot 10^6$ cycles of stresses changing.

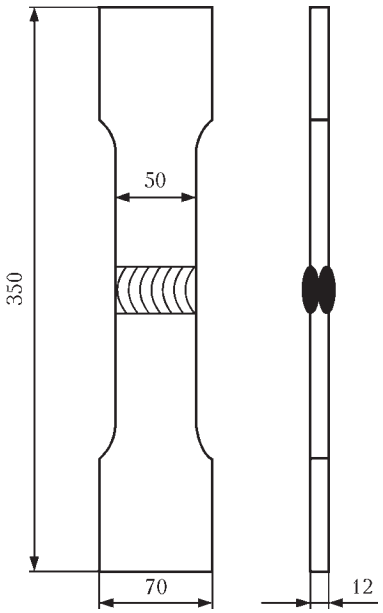

Figure 1. Shape and geometric sizes of butt welded joint specimen

The specimens were tested in the initial state and in the state strengthened by HMP after holding in a corrosive medium.

The strengthening of welded joints by HMP technology was carried out in the equipment USTREAT-1.0, in which a hand compact striking tool with a piezoceramic transducer is connected to the ultrasonic generator of an output power of 500 W. During strengthening of welded joints applying HMP technology, a narrow zone of transition of weld metal into the heat affected zone was subjected to surface plastic deformation (along the fusion line). As a strengthener, a single-row, four-needle hammer with 3 mm diameter of each hammer needle was applied. The rate of HMP during treatment of butt-welded joints was 2 mm/s, and the amplitude of oscillations of waveguide end of the hand impact tool was 25 μm.

To obtain the preliminary corrosion damages, the welded specimens were placed into the chamber KST-1. The investigations were carried out in accordance with GOST 9.401–91 «Unified system of protection against corrosion and aging. Lacquer coatings. General requirements and methods of rapid tests on resistance to climatic factors (method 1, B)» in the salt fog chamber KST-1 at a temperature of (35 ± 2) °C during spraying of sodium chloride solution for 15 min after each 45 min of investigations. The concentration of sodium chloride in the solution was (50 ± 5) g/dm^3, pH was from 6.5 to 7.2, the density was 1.03 g/cm^3. The electrical conductivity of distilled water for preparation of the sodium chloride solution was not more than 20 μOhm/cm at a tempera-

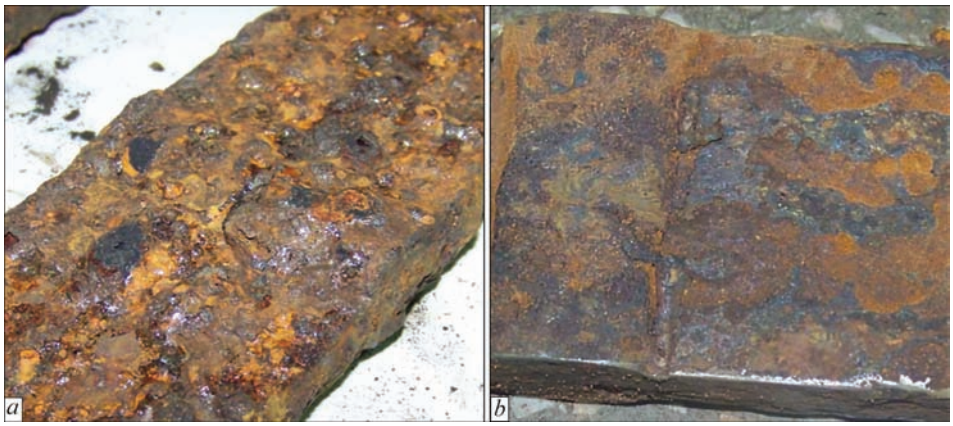

Figure 2. Appearance of weld zone of specimen of butt welded joint strengthened by HMP after holding in the KST-1 chamber for 1200 h before (*a*) and after (*b*) the partial removal of corrosion products

ture of (25 ± 2) °C. The duration of welded specimens in the conditions of effect of neutral salt fog was 1200 h.

The metallographic examinations of surface layer of weld metal and heat-affected-zone (HAZ) of butt welded joints after holding in the chamber KST-1 were performed on specimens in the initial (non-strengthened) state and in the state strengthened by HMP technology. The results of metallographic examinations of surface layer of weld metal and of HAZ metal of similar welded joints in the initial state and in the state strengthened applying HMP technology before the corrosive effect are given in the work [11].

Results of investigations. After holding in the salt fog chamber KST-1 during 1200 h, most of the specimens were covered with a continuous layer of corrosion products of 1–2 mm thickness. At the same time, on some specimens far from the weld, the areas with initial hot-rolled surface layer of light-black metal were observed, which were not subjected to corrosion. A thick layer of corrosion products prevented the visual detection of location of peening zone with a characteristic groove (Figure 2). During preparation of specimens for fatigue tests, the corrosion products were partially removed, the side edges and clamped parts of specimens were dressed to a metallic glittering. The test part of the specimens was not subjected to dressing, in the process of fatigue testing, the corrosion products were delaminated. Throughout the entire area of the specimens surface, the corrosion spots with caverns and the caverns with pitting inside were observed.

As far as fatigue cracks, as a rule, are formed along the fusion line, the corrosion damages were investigated in the transition zone of weld metal to HAZ metal.

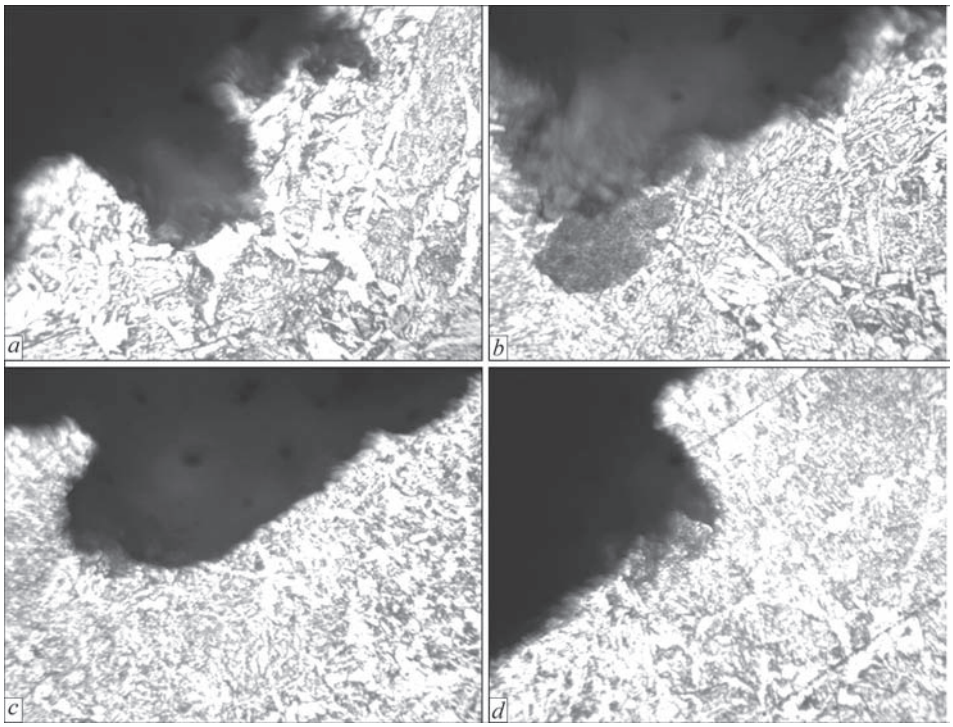

Figure 3. Corrosion damages in the fusion zone of butt-welded joint in the initial (*a*, *b*) state and in the state strengthened by HMP (*c*, *d*) after testing in the conditions of effect of a neutral salt fog for 1200 h, ×400

Dimensions of corrosion damages in the surface layers of weld and HAZ metal of butt welded joints of steel 15KhSND after holding for 1200 h in the salt fog chamber

Condition of specimens	Corrosion of surface layers of weld metal in spots			Corrosion of surface layers of HAZ metal in spots		
	Degree of damage, %	Depth of damage, mm	Sum of damaged area projection, mm	Degree of damage, %	Depth of damage, mm	Sum of damaged area projection, mm
Without strengthening	53.7	0.104–0.390	25.8	100	0.104–0.390	7.15
Strengthened by HMP	19.9	0.039–0.195	9.56	100	0.390–0.620	6.38

In the nonstrengthened welded joints, after holding in the KST-1 chamber, in the zone of transition of weld metal to HAZ metal both in weld metal and in HAZ metal (Figure 3, *a*, *b*) the corrosion damage in the form of spots and caverns of 0.104–0.390 mm diameter (Figure 1) was observed. The degree of corrosion damage of the weld and HAZ metal was 53.7 and 100 %, respectively (Table).

After strengthening by HMP the plastically deformed layers of weld metal of 1.35 mm width and of HAZ metal of 1.45 mm width were formed under the groove. In this case their depth, characterized by visible changes in the metal structure under the groove, before placing to the KST-1 chamber was 325 μm [11]. After holding of specimens of butt welded joints in the KST-1 chamber, the metal layer strengthened by HMP is not observed (Figure 3, *c*, *d*), which indicates the complete fracture (corrosion-mechanical loss) of the strengthened layer. In welded joints strengthened by HMP as compared to nonstrengthened ones after holding in KST-1, the depth of corrosion damages (spots and caverns) in the weld metal decreased to 0.039–0.195 mm, and in the HAZ metal it increased to 0.390–0.620 mm (Table). The degree of the weld and HAZ metal damage by corrosion was 19.9 and 100 %, respectively. Thus, the strengthening applying HMP technology does not lead to increase in the corrosion resistance of the metal of the zone of peening the specimens of butt welded joints in the conditions of long-term effect of the neutral salt fog.

The results of fatigue tests of specimens of butt welded joint of steel 15KhSND after holding in the salt fog chamber KST-1 are shown in Figure 4. The experimental data obtained in the work [11] on the identical welded joints without preliminary corrosion tests (obtained in the air) are also given there. The holding of specimens of butt welded joints in the salt fog chamber for 1200 h leads to decrease in the value of limited endurance of non-strengthened welded joints on the base of $2 \cdot 10^6$ cycles by 13 % (from 187 to 163 MPa), and the cyclic life in the range of $7 \cdot 10^5$–$2 \cdot 10^6$ cycles is reduced to 2 times (curves *1* and *3*, Figure 4). After KST-1, the characteristics of fatigue resistance of welded joints, strengthened by HMP technology, also decreased significantly: the value of limited endurance on the base of $2 \cdot 10^6$ cycles decreased by 35 % (from 273 to 178 MPa), and the cyclic life decreased to 30 times (curves *2* and *4*, Figure 4). Thus, applying the HMP technology allowed increasing the value of limited endurance of butt welded joints with the subsequent effect of the neutral salt fog only by 9 % (from 163 to 178 MPa), whereas their cyclic life is at the level of cyclic life of welded joints in the initial state (in air).

The obtained values of fatigue resistance characteristics of the joints strengthened by HMP technology confirm that preliminary holding of joints for 1200 h under the conditions of a neutral salt fog (imitation of influence of environmental climatic factors characteristic for the moderately cold marine climate) resulted in the complete corrosion-mechanical loss of the plastically deformed metal layer in the peening zone. The fracture of both non-strengthened welded joints as well as those strengthened by HMP after holding in the KST-1 chamber occurred along the line of weld metal transition into HAZ metal (Figure 5). The fractographic analysis of fractures revealed the significant corrosion damages of HAZ metal in the peening zone

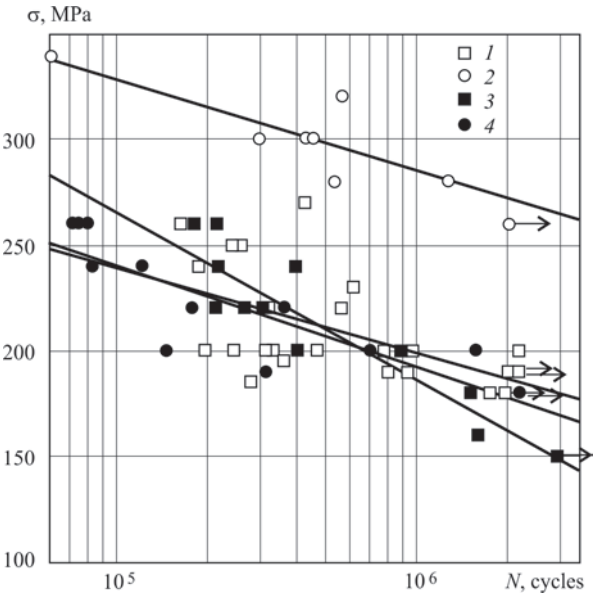

Figure 4. Fatigue curves of butt welded joints of steel 15KhSND: *1*, *2* — in the initial state and in the state strengthened by HMP technology in air [11], respectively; *3*, *4* — in the initial state and in the state strengthened by HMP technology after holding in the KST-1 chamber for 1200 h, respectively

Figure 5. General view of butt welded joint specimens strengthened by HMP technology after holding in the KST-1 chamber for 1200 h and fatigue tests

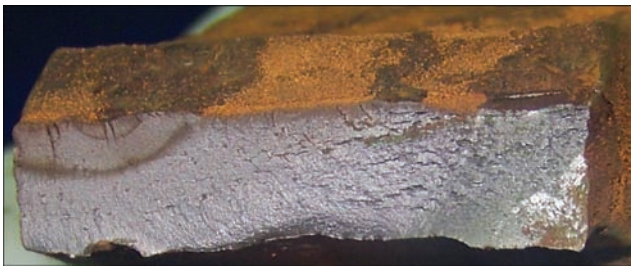

Figure 6. General view of fracture surface of the butt welded joint specimen strengthened by HMP technology after holding in the KST-1 chamber for 1200 h and fatigue tests

in the form of caverns and caverns with pittings inside (Figure 6). The initiation and propagation of cracks in the HAZ metal confirms the data of metallographic examinations (Table) of the fact, that the HAZ metal of strengthened welded joints has a lower corrosion resistance as compared to the base and weld metal.

Therefore, the experimentally obtained results indicate that in case of the long-term effect of the environmental climatic factors, characteristic for a moderately cold marine climate, a complete fracture of the surface of metal layer, plastically deformed by HMP, occurs. And, accordingly, the decrease in values of fatigue strength characteristics of welded joints occurs, strengthened to the values typical for non-strengthened joints. This can be caused by inopportune works on maintenance and restoration of protective coatings (for example, lacquer ones) of metal structure welded joints, strengthened by HMP technology.

Conclusions

1. The metallographic examinations of surface layers of the weld and HAZ metal of butt welded joints of steel 15KhSND in the initial (non-strengthened) state and in the state strengthened by HMP after corrosion tests in the salt fog chamber KST-1 for 1200 h were carried out. Based on the calculations of degree and depth, as well as the total size of projection of the area of damages by corrosion spots and caverns of surface layers of weld and HAZ metal of joints, it was established that strengthening applying HMP technology does not lead to increase in the resistance of joints against the effect of the neutral salt fog.

2. It was experimentally established that strengthening of butt welded joints of steel 15KhSND by HMP technology before holding in the neutral salt fog chamber for 1200 h does not contribute to improvement in their fatigue resistance characteristics. This is caused by the fact that preliminary holding of the joints for 1200 h in the conditions of a neutral salt fog (modeling the influence of environmental climatic factors characteristic for the moderately cold marine climate) leads to a complete corrosion-mechanical loss of the metal layer plastically deformed by HMP in the peening zone.

1. Madox, S.J., Dore, M.J., Smith, S.D. (2011) A case study of the use of ultrasonic peening for upgrading a welded steel structure. *Welding in the World*, 55(**9**), 56–67.
2. Abdullah, A., Malaki, M., Eskandari, A. (2012) Strength enhancement of the welded structures by ultrasonic peening. *Materials & Design*, **38**, 7–18.
3. Lefebvre, F., Peyrac, C., Elbel, G. et al. (2017) HFMI: Understanding the mechanisms for fatigue life improvement and repair of welded structures. *Welding in the World*, 61(**4**), 789–799.
4. He, B., Deng, H., Jiang, M. et al. (2017) Effect of ultrasonic impact treatment on the ultra-high cycle fatigue properties of SMA490BW steel welded joints. *The Int. J. of Advanced Manufacturing Technology*. DOI 10.1007/s00170-017-0608-3.
5. Malaki, M., Ding, H. (2015) A review of ultrasonic peening treatment. *Materials and Design*, **87**, 1072–1086.
6. Mikkola, E., Remes, H., Marquis, G. (2017) A finite element study on residual stress stability and fatigue damage in high-frequency mechanical impact (HFMI)-treated welded joint. *Int. J. of Fatigue*, **94**, 16–29.
7. Schubnell, J., Hardenacke, V., Farajian, M. (2017) Strain-based critical plane approach to predict the fatigue life of high-frequency mechanical impact (HFMI)-treated welded joints depending on the materials condition. *Welding in the World*, 61(**6**), 1190–1210.
8. Foehrenbach, J., Hardenacke, V., Farajian, M. (2016) High-frequency mechanical impact treatment (HFMI) for the fatigue improvement: Numerical and experimental investigations to describe the condition in the surface layer. *Ibid*., 60(**4**), 749–755.
9. Fan, Y., Zhao, X., Liu, Y. (2016) Research on fatigue behavior of the flash welded joint enhanced by ultrasonic peening treatment. *Materials & Design*, **94**, 515–522.
10. Knysh, V.V., Solovej, S.A., Nyrkova, L.I. et al. (2016) Influence of corrosion damage on cyclic fatigue life of tee welded joints treated by high-frequency mechanical peening. *The Paton Welding J.*, **9**, 42–46.
11. Knysh, V.V., Solovej, S.A., Kirian, V.I. et al. (2017) Application of high-frequency peening to improve the performance of butt welded joints in the atmosphere of temperate climate. *Ibid*., **4**, 14–18.

Received 24.11.2017

DOI: http://dx.doi.org/10.15407/tpwj2018.02.04

EFFECT OF STRUCTURE OF JOINT ZONE OF DIAMOND LAYER WITH HARD-ALLOY SUBSTRATE OF BRAZED CUTTERS ON THEIR SERVICE LIFE

B.V. STEFANIV and **O.M. SABADASH**
E.O. Paton Electric Welding Institute of the NAS of Ukraine
11 Kazimir Malevich Str., 03150, Kyiv, Ukraine. E-mail: office@paton.kiev.ua

Service life of the drilling bits with diamond-hard-alloy cutters (DHC) is determined by value of drifting under conditions of abrasive, erosion and corrosion wear in drilling of degassing holes. Evaluation of wear and microstructure of a joint of diamond layer with hard-alloy substrate of «Syndrill» integral cutter of «Element Six» Company (Ireland) and complex cutter (ISM of NASU) of drilling bits after completion of their life was carried out in the work. It is shown that cobalt in the integral cutters is uniformly distributed in the diamond layer and its amount makes up to 2.06 wt.% in contrast to complex ones, where amount of cobalt is 4.35 wt.%. Increase of cobalt content and decrease of volume content of the diamond grains in diamond layer of the complex cutters reduce their heat and wear resistance. Porosity of complex diamond-hard-alloy cutters is 2 times more in comparison with integral «Syndrill» cutters that promote penetration of larger amount of brazing alloy elements (cooper and zinc) in a transition zone of joint of hard-alloy substrate and diamond layer. 7 Ref., 2 Tables, 6 Figures.

Keywords: *drilling bit, diamond layer, diamond-hard-alloy cutter, diamond-hard-alloy plate, hard-alloy substrate, sintered material, brazing, brazing alloy, microstructure, porosity, wear*

Life of working parts of the drilling bits, equipped with integral and complex diamond-hard-alloy cutters, depends, mainly on physical-chemical properties of diamond layer and its adhesion to hard-alloy substrate after effect on it of thermal brazing cycle as well as strength and corrosion properties of brazed joint «DHC–blade of drilling bit operating element» [1–4].

High rate of wear is caused by differences in heat expansion rate between diamond particles and cobalt as well as high temperature, which effects the kinetics of chemical reactions between cobalt and diamond particles and process of diamond layer graphitizing. Considerable difference in the coefficients of heat expansion of diamond particles $1.1 \cdot 10^{-6}$ °C^{-1} and cobalt $12.0 \cdot 10^{-6}$ °C^{-1} promotes high levels of thermomechanical stresses in a transition zone of DHC joint.

Graphitizing of diamond layer of «Syndrill» cutters of «Element-Six» Company (Ireland) is significantly accelerated at more than 800 °C temperature and for cutter of diamond-hard-alloy plate (DHP) of ISM of NASU it is more than 680 °C [2]. This results in degradation of cutting edge and rise of cutters' wear, deterioration of effectiveness of drill through tool and decrease of drifting value (Figure 1).

Aim of the work is to investigate the effect of microstructure of a joint of diamond layer with hard-alloy substrate of drilling bit DHCs on their service life.

The drilling bits tests were carried out in drilling of degassing holes at 12th western airway of L_1 bed in Donbass. Drilling was performed using electrohydraulic machine for deep hole drilling of GBH 1/89/12 type from «Deilmann-Haniel» Company (Germany) at angles of drilling to horizon from 8 to 60°. A drilling mode was the following: nominal frequency of machine spindle rotation 70–100 min^{-1}; drilling thrust 50–100 kN. Drilling of the degassing holes of up to 150 m length was carried out on a matrix rock, represented by siltstone and abrasive sand rock at uniaxial compression strength limit up to 120 MPa. Consumption of technical water for borehole cleanout and drilling tool cooling made up to 50 l/min.

The integral and complex DHCs were brazed into seats of drill bit blade with the help of silver brazing alloy BAg-1a in a temperature range 650–680 °C. After the working parts of the steel drilling bits (Figure 1) have run the specific service life, the cutters were brazed out of the blade seats. Total time of holding τ at DHC brazing temperature made τ = 90–120 s.

Investigation of the microstructure of hard-alloy substrate to diamond layer joint was carried out on metallographic sections (cross section, wear of cutting edge made around 2 mm) using scanning electron microscope LEO EVO 50 XV.P (Karl Zeiss, Germany) equipped with energy-dispersive analyzer INCA-energy 450 (Oxford Instruments, England).

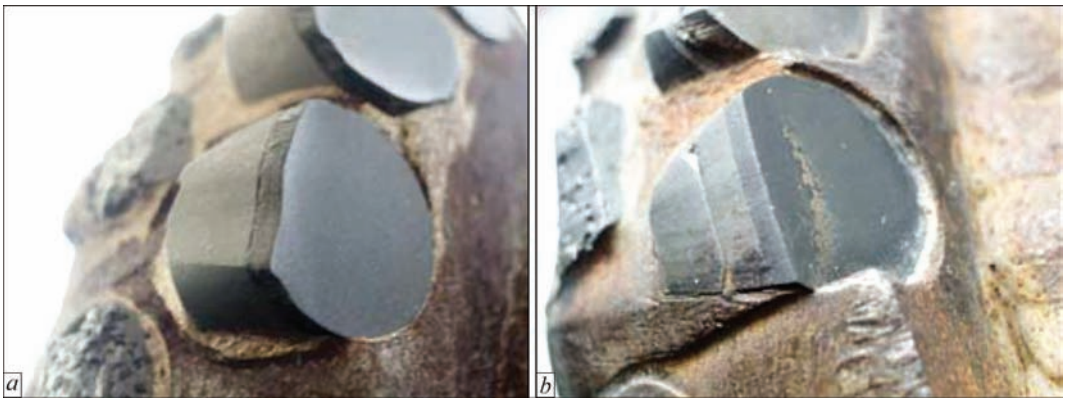

Figure 1. Appearance of worn cutters of steel drilling bit blade (×3): *a* — «Syndrill» DHC after 1000 m drifting; *b* — complex cutter of DHP of ISM of NASU after 250 m drifting

Distribution of the main elements (Figure 2) in a characteristic radiation of tungsten, cobalt, carbon indicates the presence of carbon in a diamond-containing layer (on the right) and in the segment adjacent to hard-alloy substrate (on the left) of integral «Syndrill» DHC of «Element Six» Company (Ireland). Tungsten and cobalt are located in the hard-alloy substrate and transition zone with diamond layer.

A joint of integral cutter (DHC) conventionally consists of three typical sections, namely hard-alloy substrate A, transition zone B, C, D, diamond layer E, which differ by inhomogeneous microstructure (Figure 3) and various chemical composition (Table 1).

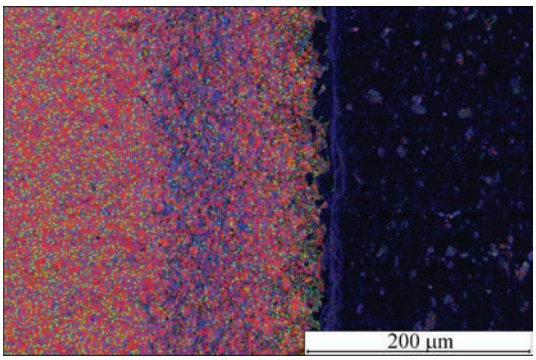

Figure 2. Distribution of elements of «Syndrill» DHC in characteristic radiation: carbon — blue, tungsten — red; cobalt — green

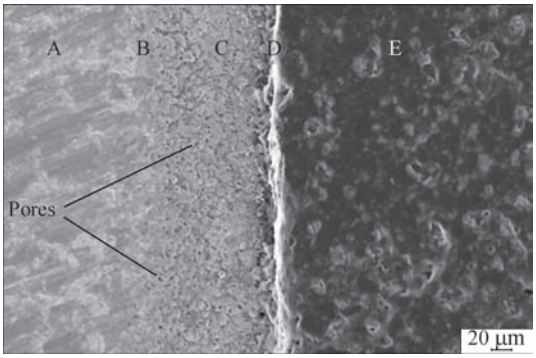

Figure 3. Microstructure of «Syndrill» DHC: A — hard-alloy substrate, (B, C, D) — transition zone, E — diamond-containing layer

A hard-alloy substrate A consists of fine-dispersed particles of tungsten carbide (light grey) bound by cobalt-based alloy (grey) containing up to 1.63 wt.% of nickel. It has a microstructure typical for hard-alloy sintered material of WC–Co system. Nickel is used as a catalytic agent [5] in sintering of the fine dispersed powders.

Hard sintered material of WC–Co system (segment B, around 10 μm width) with lower amount of cobalt (2.82 wt.%) additionally contains a separate phase of copper with zinc alloy with relationship of these elements 1.7/1. Segment C of around 120 μm width (Figure 6, *a*) has more refined microstructure of tungsten carbides, matrix of which consists of sintered material of WC–Co system and additionally contains, wt.%: 1.45 Ni and 5.59 Cu. A transition zone (segment D of around 10 μm width) has a nonuniform structure of sintered material of WC–Co (light) and C–Co (dark) systems, which contains inclusions of copper with zinc alloy at relationship of these elements 0.73/1. A diamond layer (segment E) consists of grains of polycrystalline diamonds bound by cobalt-based alloy and contains wt.%: 94.96 C; 2.06 Co (dark); 2.31 W and 0.67 Ni.

Distribution of the main elements (Figure 4) in the characteristic radiation of tungsten, cobalt, carbon of DHP complex cutter (ISM of NASU) indicates the presence of carbon in the diamond layer (on the right) and lower intensity of spectrum in a segment adjacent to the hard-alloy substrate (on the left). Tungsten and cobalt are distributed in the hard-alloy substrate. Local distribution of cobalt

Table 1. Content of elements (wt.%) in examined segments of «Syndrill» DHC

Segments	C	Co	W	Ni	Cu	Zn
A	29.42	3.92	65.03	1.63	–	–
B	42.27	2.82	41.02	1.20	3.63	2.18
C	41.15	2.83	48.98	1.45	5.59	
D	89.2	1.55	4.07	–	2.18	3.00
E	94.96	2.06	2.31	0.67	–	–

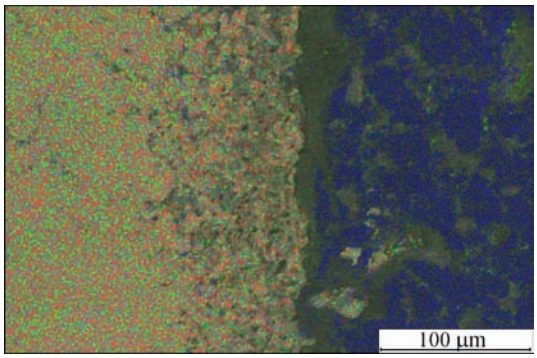

Figure 4. Distribution of elements of DHP (ISM of NASU) in characteristic radiation: carbon — blue, tungsten — red; cobalt — green

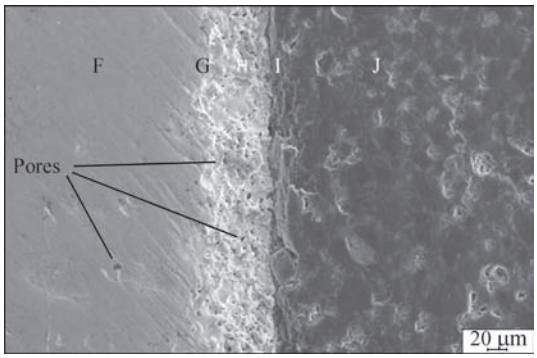

Figure 5. Microstructure of complex DHP (ISM of NASU): F — hard-alloy substrate, (G, H, I) — transition zone, J — diamond layer

(green spectrum) was determined in the segment of transition zone with diamond layer.

The joint of complex cutter, by analogy with previous DHC, consists of three typical segments different by inhomogeneous microstructure (Figure 5) and various chemical composition (Table 2).

Hard-alloy substrate F includes coarser particles of tungsten carbide (light grey) in a cobalt matrix (grey). It is similar by structure to commercial sintered material and on chemical composition it is close to VK12 alloy. Cobalt matrix G of the sintered material of WC–Co system of around 10 μm width with relatively lower amount of cobalt 9.16 wt.% additionally contains a separate phase in form of copper with zinc alloy. Segment H of around 90 μm width (Figure 6, *b*) in the transition zone is characterized by coarse grains of carbides of WC–Co system sintered material and additionally contains copper and zinc phase in relation of these elements 2.3/1. Segment I of around 10 μm width has a non-uniform microstructure typical for sintered material of tungsten carbide and diamond powders of WC–Co systems (light) and C (diamond) — Co (dark) as well as contains the inclusions of phase of copper with zinc alloy in 1.6/1 relationship. Diamond layer J contains wt.%: 89.92 C; 4.32 Co; 5.73 W.

The results of investigations showed that content of carbon naturally changes at transfer from the hard-alloy substrate to diamond layer in the separate segments, wt.%: 29.42 (A), 42.27 (B) and 41.15 (C) and rapidly rises from 89.2 (D) to 94.96 (E). Amount of cobalt (see Table 1) of DHC in the segments makes, wt.%: 3.92 (A) and 2.83 (C) and that in diamond layer 2.06 (E). Content of tungsten, on the contrary, reduces from segment A to segment E, and that in the diamond layer makes only several percent. Regularity of change of carbon and cobalt content proves complex structure of composite material of DHC consisting of sintered fine dispersed powders of the next system, namely WC–Co (hard-alloy substrate), WC–C–Co (transition zone), C–Co diamond layer.

Table 2. Content of elements (wt.%) in examined segments of DHP (ISM of NASU)

Segments	C	Co	W	Cu	Zn
F	10.48	12.22	77.30	–	–
G	19.07	9.16	65.22	4.11	2.44
H	10.46	5.36	52.99	21.8	9.39
I	67.48	7.96	13.75	6.76	4.05
J	89.92	4.35	5.73	–	–

Composition of complex DHC is also naturally varies in the separate segments, wt.%: carbon — 10.48 (F), then rises up to 19.07 (G) and reduces to 10.46 (H), and in moving across the boundary increases to 67.48 (I) and rises in the diamond layer to 89.92 (J). Amount of cobalt (see Table 2) in the segments of joint of complex DHC makes, respectively, wt.%: substrate — 12.22 (F), transition zone — 9.16 (G), — 5.36 (H), — 7.96 (I) and that in the diamond layer — 4.35 (E).

Examined segments of the transition zone of hard-alloy substrate and diamond layer of integral and complex DHC include elements from the brazing alloy, i.e. copper and zinc. A width of transition zone of hard-alloy substrate to diamond layer of integral DHC (Figure 6, *a*) is approximately 1.55 time more than of complex DHC (Figure 6, *b*).

It is known [6] that porosity of the complex domestic cutter of DHP makes 2–5 %. It can be assumed that in the processes of manufacture of complex DHP

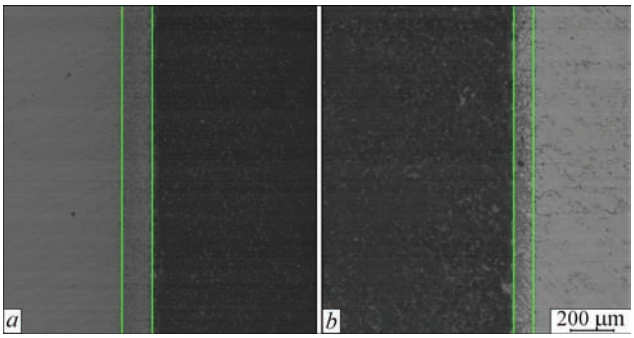

Figure 6. Microstructure of DHC with marker of width of transition zone, μm: *a* — «Syndrill», 140.6; *b* — DHP (ISM of NASU) 90.82

[2] and its fixing [3] in the holes of blades there are diffusion processes taking place in brazing, when elements of the brazing alloy, in this case copper and zinc, penetrate through the pores in the transition zone. Work [1] determined that the transition layer of hard solution based on copper with zinc is mainly formed in the near-boundary segments with hard-alloy substrate when using silver brazing alloys in the technological processes of brazing of sintered materials of WC–Co system. Porosity of domestic DHP is approximately 2 times more in comparison with DHC of «Element Six» Company (Ireland), that promotes increase of amount of copper and zinc, which forms solid solutions based on copper with zinc of alternating composition at near-boundary transition zone with hard-alloy substrate and diamond layer.

Small size WC grains and small amount of cobalt are present in the transition zone of «Syndrill» DHC in the examined segments B, C, D. They increase hardness and wear resistance due to strength. In the complex DHC G, H, I segments of the transition zones contain WC coarse grains and high content of cobalt reduces hardness and wear resistance, but rises impact toughness of the sintered alloy. Work [7] shows that coarser grains of tungsten carbides (WC) promote increase of hard alloy porosity.

Following the results of investigation of the joint of diamond layer and substrate in the specimens, produced by «Element Six» Company (Ireland) and DHP (ISM of NASU), it can be stated that the diamond layer of «Syndrill» DHC is less susceptible to effect of thermal brazing cycle and has significantly larger resource, and, respectively, value of drifting of drilling bit. High volume content of diamond grains and rigidly limited amount of cobalt binding powder in the polycrystalline DHC layer rise its strength properties, heat and wear resistance. The transition zone of «Syndrill» DHC has a relatively large dimensions, fine-grain structure of tungsten carbides (WC) and low content of cobalt as well as lower porosity in comparison with DHP (ISM of NASU). This promotes increase of hardness and relaxation of residual stresses under conditions of alternating loading.

Today, less porous sintered materials of WC–Co system are produced by means of introduction of the fine particles of tungsten carbide in a cobalt matrix and using a method of high-temperature synthesis in vacuum or in hydrogen atmosphere. Change of cobalt content and size of fine-dispersed particles allows receiving tens of standard classes of solid sintered alloys. These complex materials combine hardness at limited deformation with strength and resistance to crack formation.

Conclusions

1. Drilling bits, equipped with the integral cutters, have larger (4 times) service life in comparison with complex cutters, due to high volume content of diamond grains and limited amount of binding cobalt in the polycrystalline layer.

2. Copper and zinc components of the brazing alloy are present in the segments of transition zone adjacent to hard-alloy substrate and diamond layer. Higher porosity of complex DHC promotes increase of amount of Cu–Zn system alloy.

1. Khorunov, V.F., Stefaniv, B.V., Sabadash, O.M. et al. (2012) Peculiarities of restoration technologies of drill bits with diamond-hard-alloy cutters. In: *Problems of life and safety of service of structures, constructions and machines*: Transact. of 2010–2012 results. Kyiv, PWI, 488–493 [in Russian].
2. Stefaniv, B.V. (2013) Development of the technology of brazing of diamond-hard-alloy cutters. *The Paton Welding J.*, **2**, 37–41.
3. Stefaniv, B.V. (2013) Peculiarities of induction brazing of diamond-hard- alloy cutters to blade of body of complex drill. *Ibid*., **8**, 49–53.
4. Stefaniv, B.V., Khorunov, V.F., Sabadash, O.M. et al. (2015) Peculiarities of restoration technology for worn working parts of steel and matrix bodies of drilling bits. In: *Problems of life and safety of service of structures, constructions and machines*: Transact. of 2013–2015 results. Kyiv, PWI, 688–696 [in Russian].
5. Chintamaneni, V., Bellin, F. (2013) *High-temperature treatment at high heating rate of pdc cutters*. Pat. 2628593, RU, Int. Cl. C21D 9/22, E21B 10/567 [in Russian].
6. Goncharenko, I.M. Physical basics of development and manufacture of hard alloys. http://portal.tru.ru
7. Besson, A., Burr, B., Dillard, S. et al. (2000) On the cutting edge. *Oilfield Review*, 12(**3**), 36–57.

Received 29.11.2017

DOI: http://dx.doi.org/10.15407/tpwj2018.02.05

ELECTRIC ARC WELDING AND SURFACING IN REPAIR OF RAILS OF KYIV UNDERGROUND

G.V. KUZMENKO[1], **V.M. TAGANOVSKY**[1] and **V.L. SIDORENKO**[2]
[1]E.O. Paton Electric Welding Institute of the NAS of Ukraine
11 Kazimir Malevich Str., 03150, Kyiv, Ukraine. E-mail: office@paton.kiev.ua
[2]CE «Kiev metro»
20-a Borispolskaya Str., 02093, Kyiv, Ukraine. E-mail: C.Sidorenko@metro.kiev.ua

Operation of underground lines has own peculiarities. The most critical element of track is the rails, in which joints are particularly stressed place. Decrease of number of bolted joints significantly reduces the probability of defect formation in the rails. Experience of the E.O. Paton Electric Welding Institute on application in Kyiv underground of a new method of rails joining, namely automatic consumable electrode electric arc bath welding, is presented. It provides high productivity of welding in comparison with alumothermal welding and required mechanical properties of the joints. Restoration of surface of the rails and parts of crossing pieces is recommend to be performed using semi-automatic arc surfacing with self-shielded flux-cored wire. 4 Ref., 1 Table, 3 Figures.

Keywords: *arc bath welding, arc surfacing, rail joints, restoration of rail surface*

In modern Kyiv transport infrastructure the underground is the most reliable type of transport capable to transport the maximum number of passengers per unit of time. It covers more than 50 % of total volume of city passenger operations. Today Kyiv underground takes 24th place in the world on traffic flow, at that being only 49th on line length. Up to 2017 the Kyiv underground has three acting lines, the total operation length of which is 69.65 km with 52 stations and average daily passenger operations exceed 1.3 mln of people [1].

Kyiv underground is a multiline enterprise, modern engineering complex. 11 maintenance services, 3 electrodepots (TCh-1 «Darnitsa», TCh-2 «Obolon» and TCh-3 «Kharkovskoe»), car-repair plant (CRP), board of directors on underground construction act as its constituents.

Arrangement of track, conditions of its operation and peculiarities of interaction of track and rolling rock on underground lines significantly differ from the same on main railway transport.

Railway track in the Kyiv underground is mainly located in the tunnels with small extension of the main tracks on the surface (around 9 %). Length of spans between the stations makes from 1.0 to 2.5–3.0 km that is far less in comparison with main railways, where length of the spans usually makes from 6.0 to 10–15 km and more. Such a density of station location is caused by the need of development of traffic flows under conditions of dense urban development.

Operation conditions on the underground lines are sufficiently intensive, i.e. at relatively small axial loads on rails (static load P_s = 150 kN, dynamic P_d = = 172 kN) the average traffic density approaches and, in some cases, exceeds the average traffic density of the main railways (for example, in Kyiv underground the average traffic density reaches D_{av} = 25.23 mln of ton-kilometer/km gross per year, when on the main lines of «Ukrzaliznytsya» (UZ) this index makes 17–17.8 mln ton-kilometer/km gross per year, and on the main tracks of main lines of UZ it is 35–45 mln ton-kilometer/km gross per year). At that, intensity of trains traffic in the underground during «rush-hours» reaches 40 pairs of trains per hour, and on average 352 pairs of trains per day, which significantly exceeds this index for tracks of the main railways. Train speeds reach 70–80 km/h that is close to speed of freight and suburban trains on the mainline transport.

The rails are the main and the most critical element of a track structure. The rails are designed for guiding the wheels of rolling stock, directly accept, distribute and transfer load from the wheels to a rail seat.

Places of joining of rails between each other are called joints. By structure there are temperature, insulating and welded joints.

The gaps in the temperature joints between the rails, connected by bars, are left for having a possibility to change of a rail length at temperature variation. There is a fracture of elastic rail line and additional impact-dynamic effect of wheels on the track as a result of break of integrity and change of bending stiff-

Figure 1. Set of pilot equipment for automatic arc surfacing of rails with flux-cored wire

ness of trackway in the bolted joints during passing of the rolling stock wheels. Therefore, the joint is the most stressed place of the track. Around 35–50 % of labor expenses on track maintenance are related with joints presence. Besides, significant part of all rail defects, which appear in process of their operation, propagates mainly in a joint region. Respectively, decrease of amount of bolted joints by their replacement for welded ones as a result considerably reduces intensity of defect formation in the rails in the process of their operation.

E.O. Paton Electric Welding Institute of the NAS of Ukraine has proposed a new method of rail welding, i.e. automatic consumable electrode electric arc bath welding for replacement of bolted joints [2]. This method provides higher properties of welded joints than traditional manual arc and alumothermal welding, and has already found application in welding of tram and crane tracks [3].

Since a rail surface in the joint region is subjected to higher wear than the whole working surface of rails, which significantly longer preserves its service properties, restoration surfacing of separate areas of rail track elements is cheaper than replacement of them by new elements.

Figure 2. Automatic consumable electrode electric arc bath welding in the tunnel of Kyiv underground

Repair of rails is one the most economic methods of their service life extension. It is carried out in the process of operation without their removal from the track as well as with removal at different operations, at that first variant is more preferable from economy point of view.

The most popular and universal method of repair and restoration of rail worn surfaces and parts of crossing pieces is surfacing. Railway surfacing is widely used as a mean for extension of service life of rails and other metallic elements of the track structure [4]. Traditionally, manual electric arc welding with coated electrodes has been used for these purposes for long years. This method is successfully enough used in the cases where the volumes of repair works are relatively small, and, in the places, where access to repair zone is complicated. In the same place, where the volumes are impressive, a semi-automatic electric arc surfacing using self-shielded flux-cored wire is used.

The specialists of the E.O. Paton Electric Welding Institute of the NAS of Ukraine and line, tunnel construction and building service of CE «Kiev metro» proposed to use automatic electric arc surfacing with self-shielded flux-cored wire for repair of underground rails. It has a series of advantages in comparison with manual electric arc surfacing with stick electrodes and semi-automatic surfacing, namely high labor efficiency, culture of production and quality of surfacing operations. Since the process is continuous, number of the defects in the deposited metal and near-weld zone is reduced to the minimum, consumption of welding consumables is cut down dramatically, time for mechanical treatment of area restored by surfacing is decreased and no preheating is necessary, that shortens total time of repair.

During 2013–2015 members of the E.O. Paton Electric Welding Institute together with line, tunnel construction and building service of CE «Kiev metro» carried the investigations and experimental works in scope of complex program of the NAS of Ukraine «Problems of life and safety of service of structures, constructions and machines». The aim of these works was development of surfacing technology for rail defect repair and elimination of temperature bolted joints using automatic arc welding under conditions of acting underground tracks. A pilot equipment (Figures 1, 2) different by high mobility, necessary for performance of active repair operations, including under tunnel conditions, was developed and manufactured.

Based on agreed specifications a necessary technical documentation was developed, namely Technical regulations «Performance of pilot works on recon-

Results of three-point bending tests of reference specimens of rail joints

Zone of tension of full-scale specimens on 1 m span	Fracture loading for rails of type, kN		Bending deflection, mm
	R50	R65	
Base (loading on head) Head (loading on base)	–	1650 1380	–
Base (loading on head) Head (loading on base)	1160 860	–	22 15

struction of track elements using electric arc surfacing with flux-cored wire on Kyiv underground tracks» and «Performance of pilot works on elimination of temperature joints of rails using automatic consumable electrode electric arc bath welding on Kyiv underground tracks». Also the reference specimens of rails R50 and R65 were welded under laboratory conditions. The rails were provided by Kyiv underground. They passed three-point transverse bending tests at Kyiv rail welding enterprise of the track service of South-West railway. The results of tests (Table) corresponded to the Regulation requirements.

In November–December 2016 five joints of R50 rails and ten joints of R65 rails were welded on underground sections of all three lines of Kyiv underground, and in 2017 repair of 9 defects in form of chipping and delaminations of metal in the joints (code of defect 17.1 on TsP/0061 «Classification and catalogue of defects and damages of rails in Ukrainian railways») was performed on the underground and open sections. Indicated type of defect (Figure 3) is one of the most widespread (around 16 % from total number of rail defects on acting tracks of Kyiv underground).

Now the welded joints and repaired rails are in pilot operation and pass regular visual and ultrasonic control. The results of operation will be considered

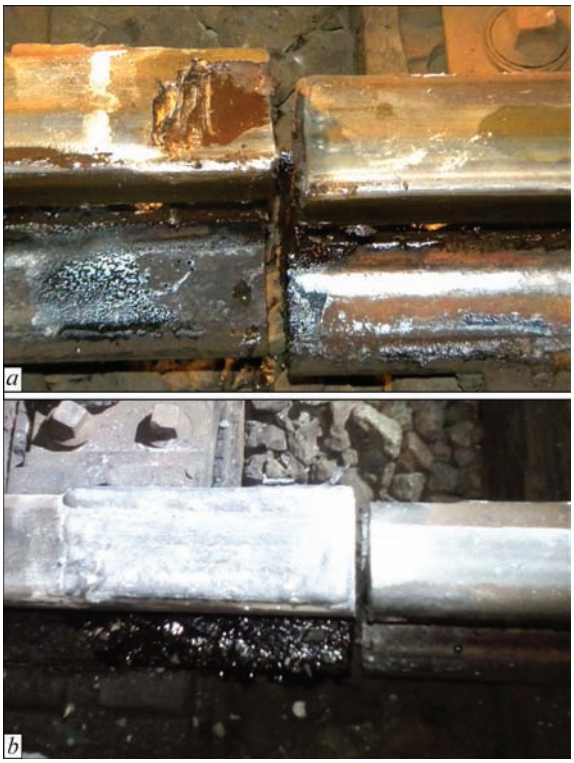

Figure 3. Rail defect 17.1 (*a*) and appearance of rail after surfacing (*b*)

in development of the documentation necessary for further commercial implementation of indicated technologies in repair of Kyiv underground tracks.

1. *Kiev metro*. http://www.metro.kiev.ua [in Ukrainian].
2. *TU U 27.1-34867717-001:2012*: Automatic consumable electrode arc bath welding of rail joints [in Ukrainian].
3. Kuzmenko, V. G., Kuzmenko, G.V., Galinich, V.I. et al. (2012) New technology of electric arc bath welding of rails on tram and crane tracks. *The Paton Welding J*., **5**, 33–36.
4. Krejnis, Z.L., Korshikova, N.P. (2001) *Maintenance and repair of railway: Manual*. Moscow, UMK MPS Russia. ISBN 5-89035-050-1 [in Russian].

Received 10.01.2018

DOI: http://dx.doi.org/10.15407/tpwj2018.02.06

APPLICATION OF WELDING FOR RESTORATION OF CAST IRON RAILING OF THE KOTZEBUE BRIDGE IN ODESSA

V.D. POZNYAKOV, Yu.V. DEMCHENKO, A.M. DENISENKO, G.V. ZHUK and **V.B. KOZYREV**
E.O. Paton Electric Welding Institute of the NAS of Ukraine
11 Kazimir Malevich Str., 03150, Kyiv, Ukraine. E-mail: office@paton.kiev.ua

The results of evaluation of real condition of cast iron railing of the Kotzebue Bridge and the opportunity of welding application for its restoration are presented. According to the instructions SRP 2007.4.1 on carrying out restoration works on the cultural heritage objects, an expert examination of the disassembled elements was carried out, the lists of defects were compiled and the complex of investigations on identification and weldability of cast iron was performed. It was established that the peculiarities of weldability of such cast iron are predetermined by its pearlite structure, carbon content, gas saturation, penetration of corrosion products deep into base metal, low ductility, as well as tendency to formation of cementite, ledeburite and welding stresses in HAZ metal. The principles of minimizing the influence of these factors on weldability were developed. The approach to selection of welding method and welding consumables was mastered. It was established that the mechanized method of welding using self-shielding high-nickel wire of grade PANCH-11 meets mostly the specified requirements. On its basis, the technology for restoring integrity of all the main architectural and decorative elements of railing (grates, emblems and cornices) was developed and implemented under the author's supervision 7 Ref., 2 Tables, 7 Figures.

Keywords: *railing, architectural and decorative elements, pearlitic cast iron, weldability, restoration, mechanized MAG welding, self-shielding high-nickel wire PANCH-11*

The Kotzebue Bridge, one of the most famous Odessa bridges, was built in 1892 (architect Landesman S.A.) over Karantinnaya ravine, now Devolanovsky descent), connecting two regions of the Politseyskaya street (now Bunin street). Its load-carrying metal structures were manufactured in France in the workshops of Gustave Eiffel, who at that time already became famous as the creator of the highest construction in the world in 1889: the Eiffel Tower with a height of 324 m. The metal structures of the bridge as well as of the tower are made of the same materials, in the similar conditions and at almost the same time, which even motivated the citizens of Odessa to call it the younger brother of the Eiffel Tower. The assembly was carried out at the mounting site in Odessa. The general view of the bridge at the end of the 19th century is shown in Figure 1. The bridge, named after Kotzebue P.E., the last governor-general of Novorossiya, is decorated with a

Figure 1. General view of the bridge at the end of the XIX century

cast iron railing. On the special grates in the center of the panel the cast emblems of Odessa are built-in: one on each side. For its originality, the railing of the bridge was awarded the status of a cultural heritage in 1985, and in 2008 the bridge was added to the state register of immovable architectural monuments.

It was managed to follow the change in the appearance of the railing over a 125-year history on the basis of analysis of photos from the thematic publications on the Kotzebue Bridge in the city mass media, since technical documents were not preserved. Figure 2 shows the general unsatisfactory condition of the railing ensemble. The poles of the railing were protected against falling by pouring the inner cavity with concrete and installing the bracings (Figure 2, *a*), which prevented the movement along sidewalk. Most of the removable railings were almost lost, except of few ones, being cast together with grates, apparently during the postwar restoration as far back as in the middle of the 20th century. As for under emblem grates, they were reinforced by the channel bars (Figure 2, *b*) at the same period, which clearly reduced the artistic component in perceiving the masterpiece of casting art. The emblems lost their curling ornaments — volutes (Figure 2, *c*).

In 2011, the load-carrying structures of the bridge floor and the cast iron railing ensemble were recognized as emergency ones and those which need the major repairs, and therefore, the bridge was decommissioned and in June 2016 it began to be reconstructed. The reconstruction project envisaged the restoration and preservation of the original arched part, without its involving in the work of bridge structures. The transport load will be now undertaken by the new span structures, meeting the modern requirements. As for railing, then after restoration it must preserve its purpose in the previous appearance.

The OJSC «ROSDORSTROY», the general contractor for reconstruction of the Kotzebue Bridge, commissioned the E.O. Paton Electric Welding Institute of the NAS of Ukraine (PWI) to fulfill the evaluation of a real condition of railing and the possibility of using welding for its restoration with the highest possible degree of preservation of its authenticity in accordance with the requirements of the instructions [1] on restoration works at the objects of cultural heritage. In the shortest terms, it was necessary to study the design, technical and artistic state of preservation, to establish the most probable factors, causes and extent of integrity loss, to prepare the lists of defects, to carry out a complex of investigations on identification and weldability of structural cast iron, to develop technical solutions and welding technology for practical restoration tasks, as well as to realize them in restoration of damaged architectural and decorative railing elements.

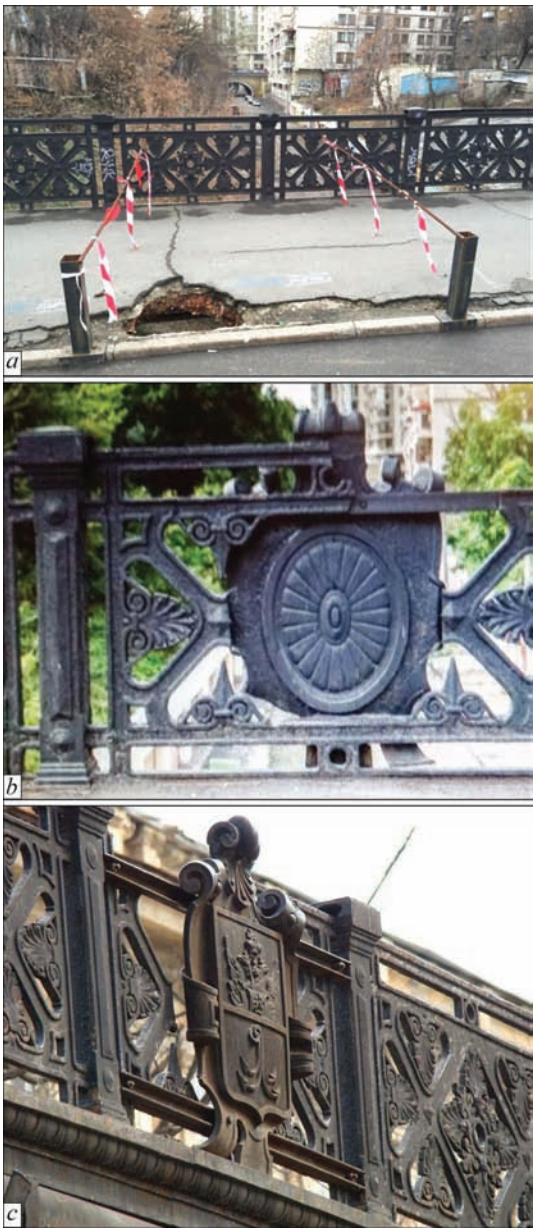

Figure 2. General view of condition of the railing of the Kotzebue bridge in 2016 (before disassembly): *a* — panoramic view; *b* — rear side of the emblem on the under emblem grate; *c* — front side of the emblem on under emblem grate

The process of disassembly of architectural and decorative railing elements was carried out manually, which did not cause a significant damage to them. The disassembled railing elements were numbered and placed in storage in the warehouse conditions of the general contractor.

In September–October 2016, under the terms of the general contractor, the first stage, an expert examination of all the architectural and decorative railing elements with element-by-element visual evaluation of a real condition and with photofixation was carried out by the specialists of the PWI (Figure 3).

To make the decisions on repairability, they were conditionally divided into two categories. To the first one the elements were attributed which are not sub-

Figure 3. Working moment of the joint expert examination of architectural and decorative elements of railing of the Kotzebue Bridge with representatives of the Department of Cultural Heritage Protection of the Odessa State Administration

jected to loading in the process of service. They are the cornices and corner elements of the decoration. To the second one the critical railing elements belong, perceiving the loads and determining the load-carrying capacity of railing: poles, grates and emblems. The applied criteria for evaluation of repairability of parts of the second category by welding were more rigid than for the parts of the first category.

During examination in both cases, a particular attention was paid to preservation of design, technical and artistic conditions. Based on the results of the examination, the lists of defects and reports of technical condition, as well as decision of repairability were drawn up. In the generalized form, the results of the examination are presented in Tables 1 and 2, and the examples of condition of some parts are shown in Figure 4.

It was established in the course of examination that the mass destruction of pillars and the loss of load-carrying capacity (Figure 4, *a*) are the results of complex cause. It consists in design features, i.e. the presence of problematic corrosion zones inside the hollow structure, low mechanical characteristics of cast iron, tight fit of grates in a standard position, vibration from transport movement, aggravated by its own weight and the weight of hinged elements, rigid action of low temperatures and water in all its aspects. The most critical for destruction is the fatigue of metal structures of the bridge in the process of long service life and corrosion. Therefore, in connection with a low degree of integrity and loss of load-carrying capacity, as well as high critical importance of these elements in the composition of the railing, it was recommended to cast all the poles anew.

The analysis showed that characteristic defects on grates (Figure 4, *b*), emblems (Figure 4, *d*) and outer horizontal surface of the cornices (Figure 4, *d*) such as cracks, lost fragments, corrosion damages are exclusively the consequences of assembly errors, action of time and long-term service. They are associated with the absence of proper current maintenance, incorrect restoration operations, unsuccessful design solutions during creation of elements, especially of under emblem grating and a low ductility of structural cast iron.

On the basis of comprehensive analysis of the degree of defectiveness of cornices, emblems and railing grates, taking into account the high degree of integrity of structural and artistic conditions, the conclusion was made about the potentiality of restoring their fitness for further service in the designing mode and in the same appearance using welding. To eliminate the design drawbacks of under emblem grates, taking into account

Table 1. List of architectural and decorative elements of the disassembled railing, presented for expert examination

Number	Description of architectural and decorative element	Quantity, pcs (account number No.)					
		Under the project	Available	Does not require repairing	Repairable by welding	Not repairable by welding	Manufacture by casting or other
1	Railing pole	44	44	3 (1, 11, 44)	–	41 (2-10, 12-43)	44
2	Railing grate (long)	40	40	29 (2-5, 7, 8, 16-19, 21-23, 25-34, 37-41, 44)	11 (1, 6, 9-15, 20, 42)	–	–
3	Railing grate (short)	4	3	1 (43)	2 (35, 36)	–	1
4	Railing grate (under emblem)	2	2	–	–	2 (24, 45)	2**
5	Railing	42	12	6 (1, 2, 3, 4, 5, 6)	–	6 (7, 8, 9, 10, 11, 12)	36
6	Corner decor element	43	43	40	3	–	–
7	Cornice (long)	42	42	35 (1-4, 6-8, 10-18, 21-26, 28-30, 32-39, 41, 45)	7 (5, 9, 19, 20, 27, 31, 40)	–	–
8	Cornice (short)	3	3	2 (42, 43)	1 (44)	–	–
9	Emblem	2	2	–	2	–	2*

Note. * — to manufacture the missing fragment by casting; ** — to manufacture completely.

Table 2. Classification of defects and content of repair of architectural and decorative elements of subrailing

Number	Description of architectural and decorative element	Characteristic defects	Content of repair, technical solutions
1	Railing poles	Corrosion and mechanical damage, loss of elements	To cast anew from gray cast iron SCh20 GOST 1412 in the quantity of 44 pcs. specified by the Project
2	Railing grates (long)	Loss of the elements of the subrailing or support girth. Cracks in the girths	Instead of the lost elements in the girths use substitute material. To weld cracks
3	Railing grates (short)	Loss of elements of subrailing and support girth. Cracks	Same
4	Railing grate (under emblem)	General destruction, loss of elements	To manufacture a new grate according to the drawing of the combined design with preservation of the original decor elements. To cast the missing decor elements
5	Railing	General destruction or loss	To cast anew from gray cast iron SCh20 GOST 1412 in the quantity of 36 pcs
6	Corner decor elements	Damages, cracks	To reweld cracks
7	Cornices (long)	Loss of fragments in the zone of mounting cuts. Cracks on the outer horizontal surface.	To use steel inserts instead of the lost fragments. To reweld cracks.
8	Cornices (short)	Loss of fragments in the zone of mounting cuts. Cracks on the outer horizontal surface.	Same
9	Emblems	Elements of curling ornament — volutes are lost.	To cast the lost elements of gray cast iron SCh20 GOST 1412 according to the drawing and to weld-on

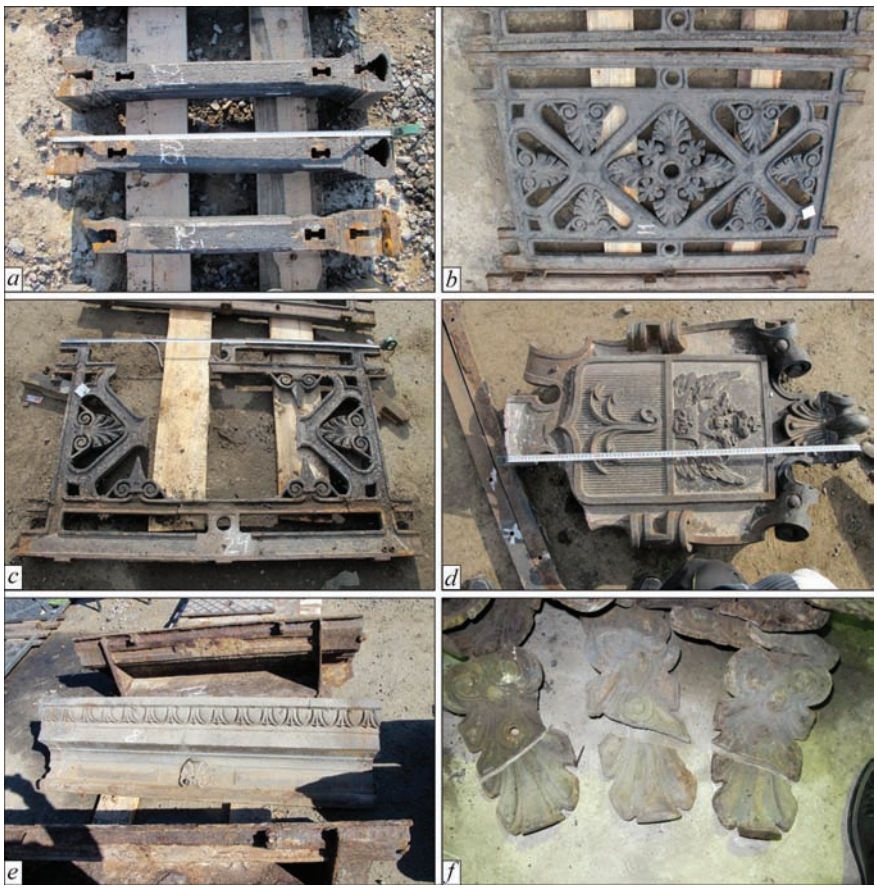

Figure 4. Examples of condition of characteristic parts of railing, established during expert examination: *a* — poles Nos 25, 26, 27; *b* — grate No. 11; *c* — under emblem grate No. 24; *d* — emblem No. 1; *e* — cornice No. 8; *e* — corner elements of decor Nos 1, 2, 3

their loading, it was suggested to restore them in the form of a combined welded-cast structure. The decision making was also contributed by the research experience in welding of gray and high-strength cast irons and participation in the restoration of cast iron pillars of the Kiev Philharmonic (19th century), pilasters of the Cabinet of Ministers building (the first half of the 20th century), as well as the load-carrying parts of technical equipment (20th century) [2].

In practice, the specialists on fracture structure determine the grade of cast iron and evaluate its weldability. In our case, fresh fractures had a fine-grained structure of light-gray color, which previously positively characterized the «French» cast iron from the point of view of weldability.

The investigation of metal samples, selected for its identification, was performed in the analytical laboratory of the Institute (Certificate of Accreditation of the National Accreditation Agency of Ukraine No. 2N362 of 14.01.2014). The composition of cast iron was determined in the X-ray spectrometer «Spectrovak-1000», the model DV-4 (Baird Company, USA), the metallographic examinations of the microstructure were performed in the optic microscope «Neophot-32» [3], the hardness was measured in the Vickers device [4]. It was established that the railing parts are cast from the cast iron of the following chemical composition, wt.%: 3.10–3.35 C; 0.37–0.40 Mn; 1.40–1.58 Si; S <0.2; P <0.15. The microstructure of cast iron of such a composition is the main factor determining the properties, as a rule it should be ferritic-pearlitic or pearlitic. According to the results of metallographic examinations, it was established that this is a typical pearlite structure in which a phosphide eutectic is present, characterized by increased hardness and brittleness. The integral hardness is not more than HV 300. As far as the decision was made to pour all the pillars and also to manufacture the railings and fragments of emblems decorations using casting anew in return for the lost ones, it was necessary to select the appropriate grade of domestic cast iron. From those, which are the closest to the original ones, a gray cast iron of grade SCh 20 meets the necessary requirements [5].

The properties of cast iron as a complex polycomponent structural material can be changed dramatically by welding process. Therefore, the technological process of welding should take into account the factors affecting weldability. All the main elements of technological process like input energy, degree of heating, cooling rate and sequence of producing joints were determined taking into account the peculiarities of the «French» cast iron and its structural transformations within the requirements [6].

Figure 5. Fragments of restoration works: *a* — restoration of under emblem grate by welding; *b* — final cleaning of welds; *c* — type of repaired joint on short cornice; *d* — type of repaired joint on grate No. 13; *e* — type of emblems before restoration (in the foreground, newly cast fragments of lost decorations — volutes); *f* — type of emblem No. 1 after restoration

The complex of investigations, carried out at the PWI, showed that the peculiar features of weldability of the «French» cast iron are predetermined not only by its structure in the fracture, but also by pearlite microstructure, carbon content, gas saturation, penetration of corrosion products into the base metal, low ductility, as well as tendency to formation of structures of cementite, ledeburite and welding stresses in the HAZ metal. For practical tasks of parts restoration, the principles were developed minimizing the influence of these factors on weldability. They consist in the fact that welding should be carried out in multilayered welds of a small length with a significant limitation of heat input and the use of welding consumables, as a rule, high-nickel ones, impeding the carbon diffusion from base metal into weld. The welding should be carried out in a narrow gap, keeping a certain sequence of its filling, without transverse electrode oscillations and it should be accompanied by layer-by-layer peening of the welds. The approach to selection of rational welding method and welding consumables was practiced. The several variants of modern welding wires and electrodes of domestic and foreign production were tested, which are necessary for welding of gray cast iron. It was established that for welding of «French» cast iron only the mechanized method of welding by self-shielding high-nickel wire of grade PANCH-11 [7] of 1.2 mm diameter (TS48-21-593–85, and only of 1987 year of production) meets mostly the specified requirements. The welded joints produced by PANCH-11 are characterized by higher resistance against near-weld cracks as compared to the joints produced by the analogues of this wire and by electrodes for manual welding with identical chemical composition of weld metal. The wire composition allows carrying out welding without preheating. At the same time, the producing of plastic austenitic weld with a hardness of not more than *HV* 200 is provided. The properties of welded joint are generally determined by the properties of base metal. In the fusion zone, a noticeable amount of ledeburite and structurally-free cementite is not observed. In the HAZ metal, there are products of non-equilibrium decay of austenite (troostite, martensite), which slightly increase the hardness to *HV* 350. Since the width of HAZ does not exceed 150 μm, its effect on properties of joints is insignificant. The composition of the wire PANCH-11 also provides a high resis-

Figure 6. General view of railing ensemble (August-September 2017): *a* — appearance of renovated panel of railing grates; *b* — under emblem grate with emblem (view from the sidewalk); *c* — view from the outside of the bridge

Figure 7. General view of the reconstructed bridge with the restored architectural and decorative railing elements (November, 2017)

tance of welds to hot cracks formation as a result of neutralizing harmful impurities and imparting a globular shape to non-metallic inclusions.

The stable process of welding using the wire PANCH-11 is easily carried out at the direct polarity and at the mode: I_w = 110–140 A, U_a = 16–18 V, which is necessary for the aims of low heat input into the base metal. The penetration depth of the base metal is 1.5–2.0 mm. The welding can be performed in all spatial positions, but the priority is given to flat and inclined positions. The weld metal is characterized by such indicators of mechanical properties as: σ_y = = 350 MPa, σ_t = 450 MPa, δ = 15 %. The specimens for static tension are fractured outside the weld metal. A significant advantage is the possibility of welding into a narrow gap in the form of a slot, which greatly facilitates the producing of joints without longitudinal and transverse cracks, as well as combined joints with steel.

Based on the results of investigations, an optimal welding repair technology was developed, applied for all architectural and decorative elements of railing, requiring restoration and a detailed plan for their restoration was elaborated, taking into account the real condition. The features of the technology are reflected in the instructions for each repair case (WPS) according to the requirements of GOST 30430–96 to the process of welding cast iron. The results of restoration works are shown in Figures 5, 6. In August 2017, after primer painting, the restored railing was installed on the Day of the City, celebrated in September, on the reconstructed Kotzebue Bridge, and subsequently in November, after the completion of the entire complex of finishing works at the adjacent territory and installation of lanterns, all the metal structures were repeatedly sand blasted and painted in the color specified by the Project (Figure 7).

Finally, it should be noted that during preparatory and restoration works of the entire set of architectural and decorative railing elements of the bridge, a number of errors and omissions were eliminated, committed during creation as well as during restoration in the past years and, applying the appropriate design and technical solutions as well as modern welding technologies and consumables, they were made as very reliable railing elements. The main principle followed by the specialists was the maximum preservation of authenticity and load-carrying capacity of the restored elements. The desired result was achieved due to the business and constructive cooperation of the organizer and the participants of the Project, as well as the advisory support of the Department of Cultural Heritage Protection of the Odessa State Administration.

1. SRP-2007.4.1. Pt 4.1: *Recommendations for performance of restoration works on objects of cultural heritage — monuments of monumental sculpture*. 4th ed. [in Russian].
2. Demchenko, Yu.V., Denisenko, A.M. (2011) Recovery of serviceability of versatile thick-wall parts from cast iron in metro equipment. *Svarshchik*, **3**, 6–9 [in Russian].
3. (2005) *GOST 344–87*: *Foundry goods with different shape of graphite. Methods of determination of structure* [in Russian].
4. (1993) *GOST 2999–75*: Metals and alloys. *Method of Vickers hardness measurement* [in Russian].
5. (1987) *GOST 1412–85*: *Spheroidal graphite iron for castings. Grades* [in Russian].
6. (1996) *GOST 30430–96*: *Arc welding of structural cast irons. Requirements to technological process* [in Russian].
7. (1987) TU 48-21-593–85: *Welding wire from PANCh-11 alloy. Specifications* [in Russian].

Received 24.01.2018

DOI: http://dx.doi.org/10.15407/tpwj2018.02.07

APPLICATION OF THE METHOD OF MICROPLASMA SPRAYING FOR MANUFACTURING RESISTANCE HEATING ELEMENT

Yu.S. BORISOV, S.G. VOJNAROVICH, A.N. KISLITSA, S.N. KALYUZHNY and **V.Yu. GLUKHOVSKY**
E.O. Paton Electric Welding Institute of the NAS of Ukraine
11 Kazimir Malevich Str., 03150, Kyiv, Ukraine. E-mail: office@paton.kiev.ua

The paper gives a description of producing a resistance heating element from multilayer coatings, which were deposited on a steel base by the method of microplasma spraying. TiO_2 in the form of powder with particles of 15–40 μm size was used to deposit narrow resistive paths. A sublayer from Al_2O_3 with 40 μm particle size was deposited to provide electrical insulation from the steel base. Performed testing of resistance heating elements showed their serviceability up to the temperature of 200 ºC at specific power of 75 W. Increase of heating temperature of resistance heating element in air above 230 ºC leads to loss of electrical conductivity. The main possible areas for such resistance heating element application are mechanical engineering, chemical and radioelectronic industries. Performed experiment allowed demonstrating the fundamental possibility of manufacturing resistance heating elements with resistive paths from TiO_2 with application of microplasma spraying technology. 18 Ref., 1 Table, 5 Figures.

Keywords: *electric heater, resistance heating element, titanium dioxide, microplasma spraying*

Electric heaters are widely used in household and industrial devices. Such electric heating devices as electrical stoves, irons, electric water heaters, electric boilers, etc. have become widely applied in the household. In industry electric heaters are used for heating chemical solutions, metal treatment furnaces; heating automatics cabinets and control stations, in manufacturing fan heaters, etc.

The main part of an electric heater is the resistance heating element (RHE). The following requirements are made of materials applied in industrial manufacture of RHE: high electrical resistance in combination with low temperature coefficient of linear expansion and high heat resistance. RHE the most widely accepted by industry are made from iron-chromium-nickel and nickel-chromium alloys of Kh23Yu5, Kh23Yu5T, Kh27Yu5T, Kh15N60 and other grades, featuring high specific resistance. Application of these materials in RHE allows using them up to 1200–1300 ºC temperatures. The next class of high-temperature RHE are batch-produced cylindrical heaters from semiconductor ceramic materials SiC, $MoSi_2$. This type of heaters is used for heating up to higher temperatures, of the order of 1500–1700 °C, compared with metal ones. Other ceramic materials, characterized by semiconductor properties, such as ZrO_2, TiO_2, TiC, Cr_3C_2, $LaCrO_3$ have also found application in RHE production [1–3]. Wide application of semi-conductor ceramic materials is due to them having higher specific resistance and smaller temperature coefficient of linear expansion than metallic ones. A design feature of metal RHE is the need for electrical insulation of the current-conducting coil from the surface being heated. An air gap is mainly used as an electrical insulator. Such a design of metal RHE leads to lowering of the coefficient of heat transfer, heat dissipation into the environment, more complicated structure and increase of overall dimensions of RHE that in some cases influences their further mounting. In order to increase the coefficient of heat transfer and reduce the overall dimensions of electric heating devices, it is possible to apply RHE in the form of resistive coatings (paths) deposited directly on the surface to be heated [4–6]. Titanium dioxide (TiO_2) is a promising material for application in RHE based on its electrophysical properties. The material has the properties of a semiconductor [7, 8] with melting temperature of 1800 °C; it is successfully used in electronics, mechanical engineering and other industries, being the most affordable semiconductor ceramic material in the market. There are also data on successful application of TiO_2 for RHE manufacturing in the form of a cylindrical roller of 540 W power [1]. Ceramics-based materials are used as electrical insulation. Al_2O_3, ZrO_2, Cr_2O_3 are the known representatives of such materials. Al_2O_3 became the most widely accepted. Its application is due to high dielectric properties at higher temperatures (5–9 kW/mm) [9] and low cost.

At present resistive paths are produced by such methods as screen printing, spreading, photolithog-

raphy, vacuum-condensate deposition, etc [4, 5]. Thermal spray technology (TST)) is considered as a promising technology among the currently-available methods of producing resistive paths. Such a technology has the following advantages: broad selection of materials, coating formation on the surface or in the local area of the item, made from practically any material, high efficiency, and simplicity of the technological process with the possibility of its automation.

Materials and equipment for coating deposition. Over the recent years TST methods allow producing coatings on different parts for radioelectronics and instrument making. There are successful results, demonstrating the possibility of their application also for manufacturing RHE [10, 11]. The main disadvantages, preventing TST application for RHE manufacturing in the currently-available equipment for thermal spraying, are great material losses at deposition of narrow resistive paths less than 6 mm wide, as well as the probability of item overheating and distortion, as a result of strong thermal impact of the plasma jet. Considering the need to form thin, narrow resistive paths, and prevent substrate distortion, it was proposed to use the technology of microplasma spraying (MPS). It allows producing coatings from different kinds of both metal and ceramic materials, significantly reducing the spraying material losses due to a small diameter of the spraying spot, thus making a minimum thermal impact on the substrate [12].

Based on the performed analysis, titanium dioxide powder with particle size of 15–40 μm and flowability of 83 s^{-1} was selected as the material to produce resistive coatings (GOST 20899–75). This material has a linear coefficient of thermal expansion of $8.19 \cdot 10^{-6}$ 1/ºC and high specific electrical resistance of $3 \cdot 10^5$ Ohm·m [13], chemical stability and electrical conductivity in oxidizing gaseous media, sufficient for resistive self-heating from room temperature. Titanium dioxide is one of the most affordable semiconductor ceramic materials in the market. Al_2O_3 powder (MRTU 9-09-3916–75) with particle size of 40 μm and flowability of 130 s^{-1} was used for deposition of electrical insulation coatings. Microplasma spraying technology was applied to increase the coefficient of spraying material utilization (CMU). This technology allows deposition of narrow-strip coatings from various kinds of materials and markedly reduces spraying material losses, owing to a small diameter of the spraying spot (3–5 mm) with minimum thermal impact on the substrate that enables producing coatings on thin-walled parts without their distortion [14, 15]. MPN-004 unit developed at PWI was used as equipment for coating deposition (Figure 1).

Figure 1. General view of MPN-004 unit

Specifications of MPN-004 unit

Working gas	Argon
Shielding gas	Argon
Plasma jet power, kW	up to 3.0
Current, A	10–60
Voltage, V	20–50
Working gas flow rate, l/min	0.5–5
Shielding gas flow rate, l/min	2–10
Efficiency, kg/h	0.1–2.5
CSMU, %	0.6–0.9
Overall dimensions, mm	500×360×50
Weight, kg	44

RHE working surfaces of 70×45×1 mm (sample No.1) and 50×50×2 (sample No.2) size were made from steel of St3 grade. Gas-abrasive treatment of the working surface was performed by fused corundum of grade A95F with F20-F22 grit size, with subsequent five minute cleaning of the surface in ULTRASONIC CLEANER PS-2 unit, using isopropylene alcohol. Dielectric strength of Al_2O_3 coatings was determined by megohmmeter F4102/1. Heating temperature influence on resistive path performance and RHE power was studied in the stand (Figure 2), consisting of

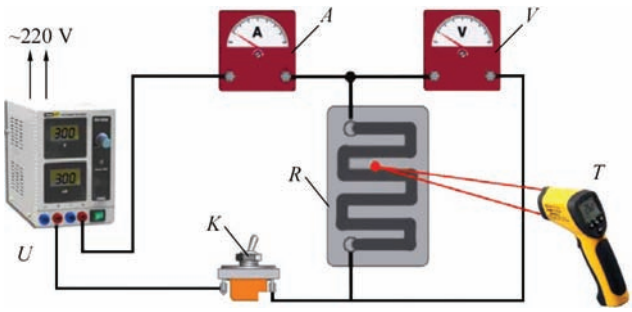

Figure 2. Schematic of the stand for studying the properties of resistive coatings: *U* is the adjustable power source; *K* is the switch for interruption of electric current supply; *A* is the ammeter; *V* is the voltmeter; *R* is the sample with resistive coating; *T* is the thermal imager (pyrometer)

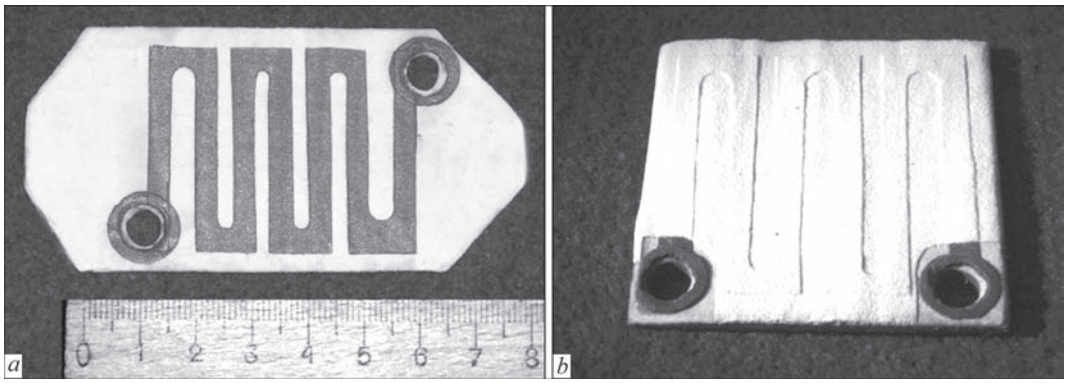

Figure 3. Resistance heating element: *a* — sample No.1 (two-layer coatings from Al_2O_3 and TiO_2); *b* — sample No.2 (three-layer coating from Al_2O_3 and TiO_2)

adjustable power source *U*, switch for interrupting electric current supply *K*, digital multimeter UNI-T UT170B for measuring current and voltage *A*, *V*, thermal imager IRISYS 1020 for measuring temperature and heat distribution through RHE *T*.

Technical characteristics of IRISYS 1020 thermal imager

Measured temperature range, °C	–10–300
Detector	pyroelectric detector 16×16
Temperature sensitivity threshold, °C	0.3
Temperature measurement error, °C, not more than	±5
Optical field of vision, horizontal×vertical, deg	20×20
Spectral range, μm	8–14
Image sweep frequency, frames, Hz	< 9
Guidance system	class 2 laser

Microstructure of TiO_2 coatings produced by MPS method, was examined in Neophot 32 microscope, porosity was determined by the method of image processing by Image Pro 3 computer program.

Manufacturing and study of resistance heating element. The process of RHE manufacturing consisted of the following stages.

1. Before deposition of electrically insulating and resistive coatings the sample bases from steel of St3 grade were subjected to liquid blasting at compressed air pressure of 7 atm. This was followed by ultrasonic cleaning of the bases to remove contamination and grease films.

2. To ensure electrical insulation of resistive paths from the metal base, MPS method was used to deposit electrical insulation layer of Al_2O_3 300 μm thick.

Mode of microplasma deposition of electrical insulation and resistive coatings

Parameters	Coating composition	
	Al_2O_3	TiO_2
Current, A	45	40
Voltage, V	30	28
Spraying distance, mm	150	150
Flow rate of working gas Ar, l/min	1.3	1.3
Flow rate of shielding gas Ar, l/min	4	4
Efficiency, g/min	1.2	2

3. After deposition of electrical insulation layer masks (from 7 spirals on sample No.1, and from 6 spirals on sample No.2) were applied on the samples to give a meander shape to the paths during spraying, with subsequent deposition of TiO_2 resistive coating by MPS method. The Table gives the parameters of deposition of electrical insulation coating and resistive paths.

4. Formed resistive paths had the following geometrical dimensions: path length on samples Nos 1 and 2 was 312 and 295 mm, respectively, path width on both the samples was 4 mm, thickness of resistive layer (TiO_2) was 150±50 μm.

5 To provide insulation of resistive paths from the environment, the same method was used to additionally deposit a layer of Al_2O_3 150 μm thick over the paths on sample No.2 (deposition modes are given in the Table). Appearance of the manufactured ceramic RHE and deposited coating microstructure are given in Figures 3 and 4.

Analysis of the microstructure of coatings (Figure 4) showed that the obtained resistive paths have a uniform thickness of 150±50 μm, electrical insulation layer (base is the resistive path) is 400±100 μm thick and external electrical insulation layer is 150±30 μm

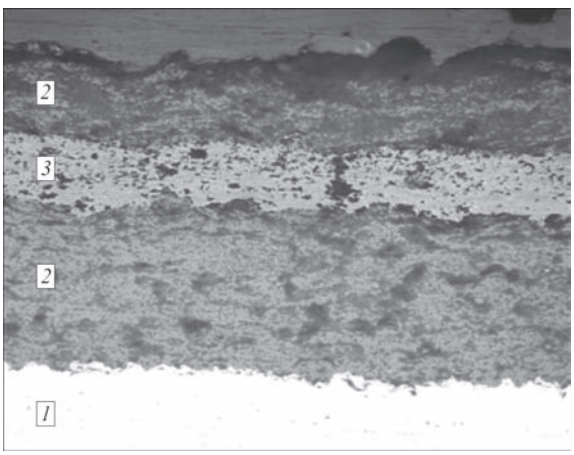

Figure 4. Microstructure (×200) of RHE three-layer coating No.2: *1* — base; *2* — Al_2O_3 layer; *3* — TiO_2 layer

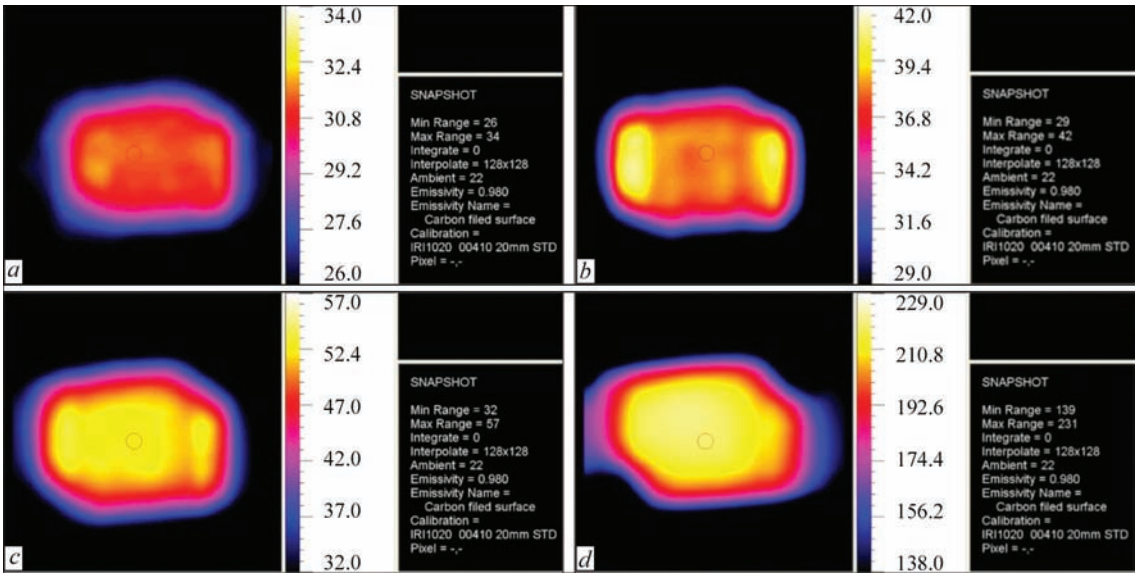

Figure 5. Heat distribution along resistive paths from TiO_2, depending on time (for *a–e* description see the text)

thick. Porosity of Al_2O_3 coatings was equal to 20–25 %, and of those from TiO_2 — 10 – 13%. Performed study of dielectric strength of electrical insulation layer from Al_2O_3 400±100 μm thick showed that it is equal to 500 MOhm at 1000 V per 6 mm^2. Obtained data are indicative of the fact that Al_2O_3 coating provides the required electrical insulation properties [16].

Electrical conductivity was studied on sample No.1, as it did not have any external protective Al_2O_3 coating that allows measuring the temperature of the resistive path directly on its surface without the impact of the external electrical insulation layer. At application of alternating voltage of 250 V to RHE current-supplying contacts, a maximum value of current of 0.3 A was obtained that corresponds to RHE specific power of 75 W. During the experiment, gradual heating of the resistive paths and heat distribution through the element took place that was recorded by IRISYS 1020 instrument (Figure 4) with 5 s time interval.

Figure 5, *a–d*, shows heat distribution through RHE according to temperature scale, recorded by IRISYS instrument. RHE initial temperature was equal to 26 °C (Figure 5, *a*). After the resistive path has reached the temperature above 230 °C, the coating lost its conducting properties.

Discussion and prospects. Conducted experiment showed the principal possibility of MPS application for RHE manufacturing using TiO_2 powders to form the resistive paths. Resistive coatings from TiO_2 produced by MPS method, allow heating the base up to 200 °C temperature without loss of RHE serviceability. Temperature increase above 230 °C, leads to local overheating of the path with loss of its electrical conductivity. Temperature limitation and conductivity loss are, obviously, due to the structure of thermal coatings, which are characterized by nonuniformity and porosity. During heating in air of resistive coatings produced by MPS method from TiO_2, coating resistance increases in the zone with nonuniform coating structure with their subsequent overheating and loss of electrical conductivity [17, 18].

These resistive coatings can be applied in practice in manufacturing RHE for protection of electric motors and generators from humidity, heating of water pumps in winter to prevent their icing, maintaining constant temperature inside electric cabinets with automatics, heating of slide valves, as well as in manufacturing special equipment for severe climatic conditions, where heating of fuels and lubricants in internal combustion engines is required.

Conclusions

1. Analysis of design features of RHE and materials used in their manufacture was performed. Materials, suitable for producing resistive paths by the method of thermal spraying were determined.

2. Possibility of manufacturing RHE by microplasma spraying method was proved experimentally. Resistive paths from TiO_2 4 mm wide with resistive layer thickness of 150±50 μm were produced.

3. Conducted testing demonstrated the serviceability of RHE manufactured by the method of MPS from TiO_2 at specific power of 75 W up to 200 ºC temperature without loss of electrical conductivity.

4. Areas of practical application of RHE with use of these coatings were determined in the instrumentation and components of equipment for mechanical engineering, chemical and radioelectronic industry.

5. Alloying, for instance with application of Cr_2O_3, can be a way to improve the working temperature and stability of electrophysical properties of the resistive path from TiO_2.

1. Scheitz, S., Toma, F.-L., Berger, L.-M. (2011) Thermally sprayed multilayer ceramic heating elements. *Thermal Spray Bull*., **2**, 88–92.
2. Baranovsky, N.D., Sharonov, E.A., Vannovsky, V.V. (1991) Electrical properties of plasma coatings for plane heating elements. *In: Proc. of Mathematical Conf. on Thermal Spraying in Industry of USSR and Abroad* (Leningrad, 27–29 May 1991). Leningrad, LD NTP, 60–61 [in Russian].
3. Dostanko, A.P., Vityaz, P.A. (2001) *Plasma processes in manufacture of electronic engineering products*. Minsk, FU AINFORM [in Russian].
4. Ivanov, A.S., Lebedev, Yu.P. (2005) *Heating block for household electric appliances*. Pat. 2246804 RF [in Russian].
5. *Heating* elements of ONIX Company. http://mef.narod.ru/nagrev.htm [in Russian].
6. Gonenko, T.V., Khatsevsky, V.F., Khatsevsky, K.V. (2010) *Engineering method of calculation of multi-track heaters*. Vestnik PGU, 3, 30–34 [in Russian].
7. Khoroshikh, V.M., Belous, V.A. (2009) Films of titanium dioxide for photocatalysis and medicine. *Fizicheskaya Inzheneriya Poverkhnosti*, 7(**3**), 223–238 [in Russian].
8. Pasynkov, V.V., Sorokin, V.S. (2001) *Materials of electronic engineering: Manual*. St.-Petersburg, Lan [in Russian].
9. Vashkevich, F.F., Spalnik, A.Ya., Pluzhko, I.A. (2009) Electrothermic insulation of inductors for internal heating of tubular billets. *In: Building, Materials Science, Mechanical Engineering*. Dnepropetrovsk, PGASA, 4–6 [in Russian].
10. Lyasnikov, V.N., Perov, V.V., Lavrova, V.N. (1977) Application of plasma-arc spraying of alundum in manufacture of cathode-heating unit. *Elektronnaya Tekhnika*. Ser. Elektronika SVCh, **4**, 85-87 [in Russian].
11. Baklanov, D.I., Belyajkov, I.N., Virnik, A.M. et al. (1996) *Method of manufacturing of resistive heating element*. Pat. 2066514 RF, Int. Cl. H 05 B 3/12 [in Russian].
12. Vojnarovich, S.G. (2012) Examination of shape and size of spraying spot and metalizing figure under conditions of microplasma spraying of hydroxyapatite coating. *Vestnik NUK*, **3**, 81–84 [in Russian]
13. Samsonov, G.V., Epik, L.P. (1973) *Refractory coatings*. Moscow, Metallurgiya [in Russian].
14. Borisov, Yu.S., Pereverzev, Yu.N., Bobrik, V.G., Vojnarovich, S.G. (1999) Deposition of narrow-band coatings by microplasma spraying method. *Avtomatich. Svarka*, **6**, 53–55 [in Russian].
15. Kislitsa, A.N., Kuzmich-Yanchuk, E.K., Kislitsa, N.Yu. (2009) Producing narrow paths by microplasma spraying method from Ni–Cr wire. *In: Abstr. of Papers of All-Ukrainian Sci.-Tekhn. Conf. of Young Scientists and Specialists on Welding and Related Technologies* (Kiev, 27–29 May 2009), 94 [in Russian].
16. *GOST 1516.1–76:* A.c. electric equipment for 3–500 kV voltage [in Russian].
17. Barabanova, E.V., Zaborovsky, K.M., Posadova, E.M., Kastro, R.A. (2013) Influence of porosity on electrophysical properties of PZT ceramics. *Izvestiya A.I.Gertsen GPU*, **157**, 79–83 [in Russian].
18. Zheglova, A.I. (1994) *Synthesis and electrical properties of oxide ceramics for application in electronics*. In: Syn. of Thesis of Cand. of Techn. Sci. Degree. Kiev [in Russian]. http://tekhnosfera.com/sintez-i-elektricheskie-svojstva-oksidnoy-keramiki-dlya-primeneniya-v-elektronike.

Received 29.12.2017

DOI: http://dx.doi.org/10.15407/tpwj2018.02.08

ELECTROSLAG SURFACING OF BILLET END FACES WITH APPLICATION OF CONSUMABLE AND NONCONSUMABLE ELECTRODES

Yu.M. KUSKOV, V.G. SOLOVIOV, P.P. OSECHKOV and **V.V. OSIN***
E.O. Paton Electric Welding Institute of the NAS of Ukraine
11 Kazimir Malevich Str., 03150, Kyiv, Ukraine. E-mail: office@paton.kiev.ua

Producing minimum and uniform penetration of base metal at electroslag surfacing of end faces by consumable electrode of a large cross-section is a complex task. The most promising is the application of nonconsumable electrode – current-supplying mould for these purposes. Influence of different electric circuits of connection of electrodes of different diameter from one or two AC power sources on base metal penetration was studied. It is found that from the viewpoint of optimizing the surfacing technology (achievement of not only quality indices, but also increased process efficiency), it is promising to apply the surfacing circuit with one power source and the same potentials on the bottom plate and current-conducting section of the current-supplying mould. Circuit of electroslag surfacing with two sources allows producing similar results, but it is more complicated to implement (presence of two sources) and less cost-effective, respectively. Obtained results can make up the data bank for designing a system of automatic regulation of base metal penetration at electroslag surfacing of end faces. 11 Ref., 1 Table, 3 Figures.

Keywords: *electroslag surfacing of end faces, large cross-section consumable electrode, current-supplying mould, AC power sources, base metal penetration*

Proposed by the staff of Donetsk National Technical University technology of electroslag surfacing of end faces, which they called bulk ESS, is quite widely accepted for reconditioning various products, mainly excavator bucket teeth. Various surfacing techniques are used, and electrodes can be both composite, and standard ones [1, 2]. As a result, the size of the transition zone cannot be greater than 300 μm [3, 4]. Obtaining small values of the transition zone often requires stringent conditions for conducting the electroslag process. In particular, in the case of, for instance, application of electroslag heating at surfacing, the metal pool depth and base and deposited metal mixing increase markedly at insufficient time of its impact [4]. Thus, the quality of single-electrode ESS in a standard water-cooled mould depends on a multitude of factors influencing the final result of surfacing.

In [5] it was shown that the required bimetal characteristics can be obtained at application of nonconsumable electrode – current-supplying mould (CSM) and one power source, but it is rather difficult to ensure the stability of its quality from one surfacing operation to another one.

As regards electroslag remelting (ESR) in CSM, in order to obtain a relatively flat metal pool the authors of [6, 7] suggest applying the so-called two-loop (two power sources) circuit of conducting the electroslag process. And even though the influence of various process parameters on reaching the posed goal is considered in sufficient detail in these works, still these data belong to the technology of producing ESR ingots. It remains unclear what position of the edge of surface-melted electrode in the slag pool should be regarded as the optimal one. In our opinion, solving this problem is the most important from the viewpoint of automation of the process of regulation of base metal penetration at ESS. Now, practical confirmation of the possibilities for application of the two-loop circuit, when producing steel-copper billets of d.c. arc furnace anodes [8] is not quite convincing, as the depth of metal pool in melting highly heat-conducting metal (copper) is relatively small [9].

Repeatability of quality characteristics of bimetal billets can be ensured by optimizing both the electrotechnical (kind of applied current, circuits of connection of consumable electrode of different diameter, number of power sources) and geometrical parameters (position of processed surface relative to CSM current-conducting section, position of consumable electrode edge relative to the processed surface).

*Engineer A.I. Evdokimov took part in surfacing experiments.

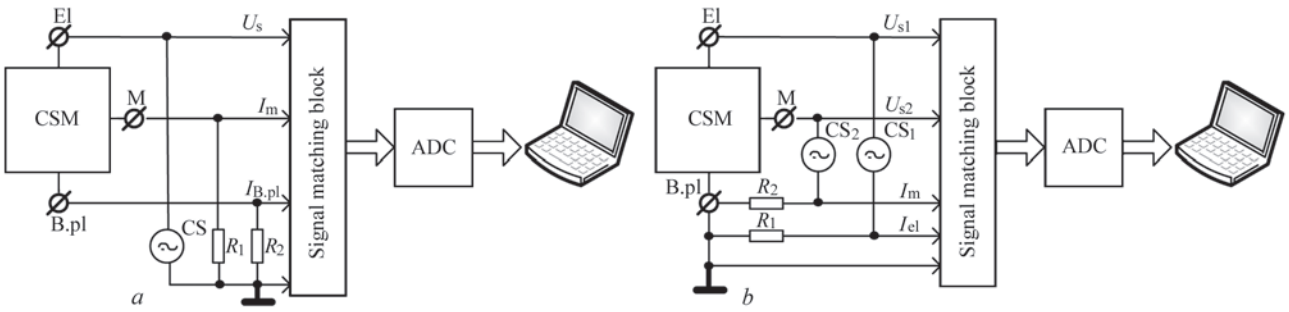

Figure 1. Block-diagram of electrical connections at performance of experiments for single-loop (*a*) and two-loop (*b*) ESS (E, M, and B.pl are the terminals for connection of the electrode, current-conducting section of the mould and bottom plate to the billet, respectively; CS is the AC source; R_1, R_2 are the instrument current shuts; U_s, I_m, $I_{b.pl}$, I_{el} are the signals proportional to power source voltage, mould current, bottom plate current and electrode current, respectively; ADC is the analog-digital converter)

This work is a continuation of earlier started research on ESS of end faces with large-section electrode in CSM [5]. The paper provides analysis and comparison of various engineering solutions from the viewpoint of cost-effectiveness of the surfacing process, simplicity of its implementation and stability of surfacing quality results. Various electric circuits of connection of electrodes of different diameter to one or two a.c. power sources are taken as variable parameters. Alternating current was selected for surfacing as the most widely accepted one in electroslag technologies [10, 11]. It is also intended to use the data obtained as a result of test surfacing performance at development of a system of automatic regulation of base metal penetration.

Surfacing experiments, similar to [5], were performed with ANF-29 flux in CSM of 180 mm diameter with 40–130 mm electrodes from steel 40. Steel St.3 billets 20 mm thick were fixed on a water-cooled bottom plate. TShP-10 and TShS-3000-1 were used as power sources.

Figure 1 shows the block-diagram of electrical connections during performance of experiments for single-loop (*a*) and two-loop (*b*) ESS. Measurement and recording of currents and voltages was conducted using a versatile ADC module E14-440 (USB2 bus), LENOVO notebook IdealPad Y650 model with 64-bit operating system and PowerGraph software (SW). Signals in the form of voltages, proportional to currents in the source circuits, were read using instrument current shunts R_1 and R_2. Voltages of current sources and signals of currents in the source circuits were entered through signal matching unit, which had the role of overload protection and high-frequency interference filter, into ADC with discretization frequency of 1.0 kHz, and then into the computer for processing. Power Graph SW was used to calculate effective values of entered signals of alternating current and voltage, and then these were stored in the computer memory. Figure 2 shows a fragment of recording the surfacing process parameters (22M experiment).

The Table gives the results of experiments on investigation of the influence of electric parameters of the process of ESS in CSM (at application of electrodes of different diameter and their connection circuits) on base metal penetration. Experimental results were used to analyze the macrosections of the produced bimetal, and calculate the average depth of billet penetration and average nonuniformity of its penetration. As an example, Figure 3 shows a macrosection of a bimetal sample (25M experiment). Dotted line denotes the zone of metal mixing.

Average penetration depth H_{av} was defined as $H_{av} = S_{up}/D_b$, were S_{up} is the macrosection surface area between the item upper level and item penetration line; D_b is the blank diameter. Average nonuniformity of billet penetration Δ_{pen} was defined as $\Delta_{pen} = S_\Delta/D_b$, where

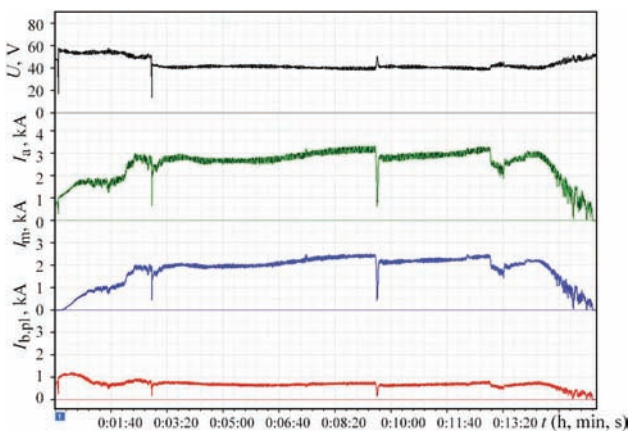

Figure 2. Fragment of recording the surfacing process parameters (22M experiment)

Figure 3. Macrosection of bimetal sample (25M experiment). Dotted line denotes metal mixing zone

ESS mode parameters and assessment of the quality of bimetal samples made in CSM

Experiment number	Electode diameter, mm	Connection circuit	Current, kA		Voltage, V		N_{tot}, kV·A	N_{CSM}/N_{el}	v_{el}, mm/min	G, kg/h	h, mm	Q, kW·h/kg	Surfacing quality		
			CSM	Electode	CSM	Electode							H_{av}	Δ_{av}	QPS
21M	130	OC	2.5	3	0	44	132	45/55	18	135	85	1	8	3	Good
22M	90	Same	2.1	2.8	0	41	115	43/57	18	50	85	2.3	7	3	Excellent
23M	40	»	1.5	2.4	0	50	120	38/62	110	34	85	3.5	3	1	Same
25M	90	TC	3.2	2.4	37	68	293	43/57	49	42	85	6.9	2	1	Good
26M	90	Same	1.2	2	42	11	72	31/69	51	10	85	7.2	4	2	Same
28M	40	»	2.6	1.6	33	40	150	43/57	76	28	85	5.4	2	1	Excellent
29M	40	»	2.3	1.2	32	42	124	41/59	89	24	61	5.2	15	8	Good

Note. OC, TC are the one-loop and two-loop circuits of CSM connection, respectively; N_{tot} is the total power consumed by CSM; N_{CSM}/N_{el} is the ratio of powers in the mould and electrode; v_{el} is the speed of electrode movement; G is the deposition efficiency; h is the distance from the processed surface to the upper edge of forming section; Q is the specific power consumption; H_{av} is the average penetration depth, mm; Δ_{av} is the average nonuniformity of penetration, mm; QPS is the quality of processed surface formation (expert assessment).

S_{Δ} is the macrosection surface area, limited by line H_{mid} and item penetration line. Quality of processed surface formation (QPS) was assessed by three experts.

Obtained data confirm that ESS with application of one-loop power circuit with the same potentials on the bottom plate and CSM current-conducting section (21M, 22M and 23M experiments) provides a higher efficiency that does the two-loop circuit of ESS with a common point of power sources connection on the bottom plate (25M, 26M, 28M and 29M experiments). This is, obviously, related to the fact that at surfacing the fraction of current flowing through the electrode is much higher in the first case than in the second one. In this connection, it is of interest to study ESS by the two-loop circuit with a common point of power sources connection on the electrode, having, supposedly, a higher efficiency, than that with a common point of connection on the bottom plate. It should be noted that the two-loop circuit of ESS with a common point of both the power sources connection on the bottom plate is the traditional circuit for application of two power sources at ESR in CSM [6–8].

For all the experiments, including also ESS by two-loop circuits, practically the same power ratio N_{CSM}/N_{el} (31–45)/(55–69) was ensured. In these experiments, similar to [6–8], ESS by a two-loop circuit with power ratio in favour of the mould, was not used, as in this case, in our opinion, the fraction of power on the electrode during surfacing is reduced, and ESS by the two-loop circuit will lead to even greater lowering of deposition efficiency, because of lowering of electrode melting rate.

Experiments showed that ESS by one-loop circuit with application of 40 mm electrode (23M experiment) can compete, in terms of such parameters as H_{av} and Δ_{pen}, with ESS by the two-loop circuit (28M experiment). Reduction of the distance from the processed surface to the upper edge of the forming section from 85 to 61 mm (28M and 29M experiments) led to a significant increase of average penetration depth (from 2 to 15 mm) and average nonuniformity of penetration (from 1 to 8 mm). This is, probably, related to increase of the degree of impact of hot molten metal on the billets. Changing electrode diameter from 130 to 40 mm led to reduction of both H_{av} and Δ_{pen}.

Conclusions

1. The possibility of performance of end face ESS with various electric circuits of connection of electrodes of different diameter from one or two AC power sources was established, and the influence of electric and process parameters on base metal penetration was studied.

2. It is shown that the surfacing circuit with one power source and the same potentials on the bottom plate and current-conducting section of CSM (nonconsumable electrode) can be considered promising, from the viewpoint of producing an optimum surfacing technology (achievement of not only quality indices, but also increased process efficiency).

3. ESS circuit with two sources allows producing results similar to those at ESS with one power source, but it is more complex to implement (presence of two sources), is characterized by lower efficiency and accordingly, is less cost-effective.

4. It seem promising to study ESS by a two-loop power circuit with a common point of connection of both the sources on the electrode, having, supposedly, a higher efficiency that the circuit with a common connection point on the bottom plate.

5. Obtained results can make up a data bank for development of a system of automatic regulation of base metal penetration at end face ESS.

1. Shvartser, A.Ya., Dorokhov, V.V, Ponomarenko, V.P. (1982) Development of electroslag surfacing method of excavator

bucket teeth. In: *Modern methods of surfacing and their application*. Kiev, PWI, 70–77 [in Russian].
2. Kiseleva, I.V., Dorokhov, V.V., Shvartser, A.Ya., Gerasimov, E.A. (1989) Application of electroslag heating in hardening restoration surfacing of excavator bucket teeth. *Problemy Spets. Elektrometallurgii*, **3**, 28–30 [in Russian].
3. Ponomarenko, V.P., Shvartser, A.Ya., Stroganova, G.V. (1985) Examination of fusion zone of high-chromium cast iron with high-manganese steel in electroslag surfacing. *Metallovedenie i Term. Obrabotka Metallov*, **11**, 55–58 [in Russian].
4. Kiseleva, I.V., Dorokhov, V.V., Schvartser, A.Ya., Gerasimov, E.A. (1989) Regulation of extension of transition zone by electroslag heating method. *Problemy Spets. Elektrometallurgii*, **4**, 15–19 [in Russian].
5. Kuskov, Yu.M., Soloviov, V.G., Zhdanov, V.A. (2017) Electroslag surfacing of end faces with large-section electrode in current-supplying mould. *The Paton Welding J.*, **12**, 29–32.
6. Tsykulenko, A.K., Lantsman, I.A., Medovar, L.B. et al. (2000) Two-circuit electroslag remelting of consumable electrode. *Problemy Spets. Elektrometallurgii*, **3**, 16–20 [in Russian].
7. Medovar, L.B., Tsykulenko, A.K., Chernets, A.V. et al. (2000) Examination of influence of two-circuit ESR parameters on sizes and shape of metal pool. *Ibid*., **4**, 3–7 [in Russian].
8. Zajtsev, V.A., Medovar, L.B., Tishchenko, P.I. et al. (2011) Application of two-circuit ESR for producing of steel-copper anode billets of d.c. arc furnaces. *Sovrem. Elektrometall*., **2**, 3–7 [in Russian].
9. (1986) *Metallurgy of electroslag process*. Ed. by B.E. Paton, B.I. Medovar. Kiev, Naukova Dumka [in Russian].
10. (1976) *Electroslag furnaces*. Ed. by B.E. Paton, B.I. Medovar. Kiev, Naukova Dumka [in Russian].
11. (1980) *Electroslag welding and surfacing*. Moscow, Mashinostroenie [in Russian].

Received 15.11.2017

LASER TECHNOLOGY AND EQUIPMENT FOR

MANUFACTURE OF MULTILAYER BELLOWS

PWI has developed the technology and equipment for laser welding of thin-wall pipes of stainless steel for manufacture of multilayer bellows, which carry and divide liquid and gaseous media, including aggressive ones.

Following the developed technology the bellow consists of several laser-welded thin-wall pipes (from 3 to 10 layers) of 0.15–0.20 mm thickness each. The bellow will keep working capacity in such a multi-layer bellow structure, even if one welded joint breaks in process of operation.

Development advantages:

- reduced amount of rejects from 50% in argon-arc welding to 0.5 % in laser welding
- 4 times rise of productivity
- cyclic strength, corrosion resistance and other characteristics of laser-welded multilayer bellow 1.5–4 times exceed the characteristics of single layer bellow made by argon-arc welding (depending on number of layers and bellow sizes).

Developed by the E.O. Paton Electric Welding Institute of the NAS of Ukraine. E-mail: office@paton.kiev.ua

UNIT FOR
MANUAL LASER WELDING

PWI by the order of carriage works (Changchun, China) has developed the unit for manual laser welding of car elements of modern high-speed trains. Weight-dimensions characteristics of the developed tool allow welding in different spatial positions. Carried metallographic investigations and mechanical tests of the welds produced with developed manual laser tool showed that the level of mechanical characteristics of given welded joints are as good as characteristics of the joints made using automatic laser welding.

LASER WELDING
OF BODY ELEMENTS WITH LOOSE EDGES

A technology for brazing of body elements of filters of 0.5–0.6 mm thickness stainless steels for paints and lacquers was replaced with laser welding using filler material in form of metallic powder. As a result, amount of defective products became 10 times smaller (spoilage in laser welding is 0.5 %). Strength and corrosion resistance of the joint is on the level of body base metal.

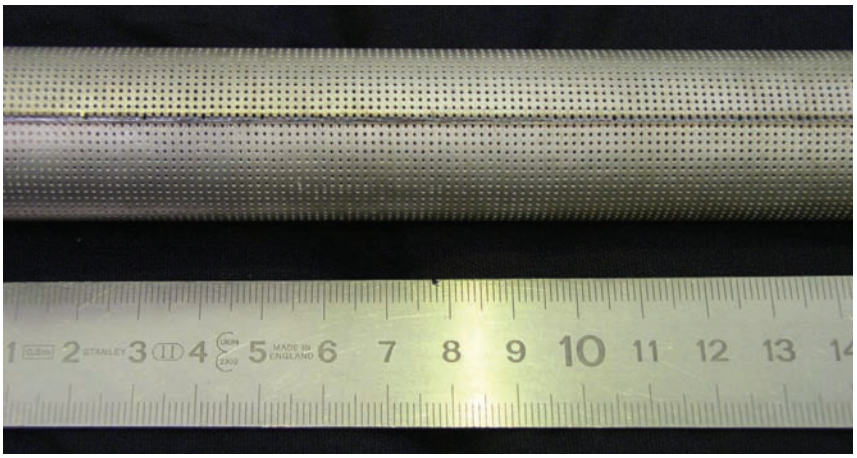

Developed by the E.O. Paton Electric Welding Institute of the NAS of Ukraine. E-mail: office@paton.kiev.ua

PATON PUBLISHING HOUSE

www.patonpublishinghouse.com

SUBSCRIPTION

«The Paton Welding Journal» is Published Monthly Since 2000 in English, ISSN 0957-798X, DOI: http://dx.doi.org/10.15407/tpwj.

«Avtomaticheskaya Svarka» Journal (Automatic Welding) is Published Monthly Since 1948 in Russian, ISSN 005-111X, DOI: http://dx.doi.org/10.15407/as.

«The Paton Welding Journal» is Cover-to-Cover Translation of «Avtomaticheskaya Svarka» Journal into English.

If You are interested in making subscription directly via Editorial Board, fill, please, the coupon and send application by Fax or E-mail.

The cost of annual subscription via Editorial Board is $348 for «The Paton Welding Journal» and $180 for «Avtomaticheskaya Svarka» Journal.

«The Paton Welding Journal» can be also subscribed worldwide from catalogues subscription agency EBSO.

SUBSCRIPTION COUPON

Address for journal delivery _____

Term of subscription since _____ **20** **till** **20**

Name, initials _____

Affiliation _____

Position _____

Tel., Fax, E-mail _____

We offer the subscription all issues of the Journals in pdf format, starting from 2009.

The archives for 2009–2016 are free of charge on *www.patonpublishinghouse.com* site.

ADVERTISEMENT

in «Avtomaticheskaya Svarka» and «The Paton Welding Journal»

External cover, fully-colored:
First page of cover (190×190 mm) — $700
Second page of cover (200×290 mm) — $550
Third page of cover (200×290 mm) — $500
Fourth page of cover (200×290 mm) — $600

Internal cover, fully-colored:
First/second/third/fourth page of cover (200×290 mm) — $400

Internal insert:
Fully-colored (200×290 mm) — $340
Fully-colored (double page A3) (400×290 mm) — $500

- Article in the form of advertising is 50 % of the cost of advertising area
- When the sum of advertising contracts exceeds $1001, a flexible system of discounts is envisaged

Size of journal after cutting is 200×290 mm

Editorial Board of Journals «Avtomaticheskaya Svarka» and «The Paton Welding Journal»
E.O. Paton Electric Welding Institute of the NAS of Ukraine
International Association «Welding»
11 Kazimir Malevich Str. (former Bozhenko Str.), 03150, Kiev, Ukraine
Tel.: (38044) 200 60 16, 200 82 77; Fax: (38044) 200 82 77, 200 81 45
E-mail: journal@paton.kiev.ua; www.patonpublishinghouse.com